AN INVESTIGATION OF
SYSTEM IDENTIFICATION WITH ECCENTRIC MASS SHAKERS

by
Umut Karacadağlı
B.S., in C.E., Boğaziçi University, 2010

Submitted to the Institute for Graduate Studies in
Science and Engineering in partial fulfillment of
the requirements for the degree of
Master of Science

Graduate Program in Civil Engineering
Boğaziçi University
2010

ACKNOWLEDGEMENTS

I would like to acknowledge many people who have immensely helped me in the completion of this thesis. First and foremost, I would like to express my gratitude to my advisor Assoc. Prof. Hilmi Luş for his guidance and his invaluable comments through this process. I am deeply indebted to him for his genuine support, encouragement and patience. I also thank Associate Prof. Nilüfer Özyurt for providing me a space in Boğaziçi University.

I would also like to thank Assistant Prof.Serdar Soyöz and Prof. Ali Rana Atılgan for participating in my thesis committee and for their creative remarks and suggestions. I am also grateful to Bilge Alıcıoğlu for her invaluable helps and comments during this study.

I am grateful to my colleagues Emin Çiftçi, Musa Rahmanlar and Yusuf Eşidir who were always available when I needed help. I would also thank to rest of my colleagues with whom I shared a considerable amount of cheerful time.

I deeply owe to my parents Birgül and Halil, to my brother Ümit and my small brother Bawer for their love and support; I am grateful to them for believing in me, and I cannot find words to express what they mean to me…

My special thanks go to my friends Harun, Murat, Kemer and all my friends who listened my boring thesis stories patiently for years. I also would like to thank Hazalana restaurant and Adil abi for providing delicious food everyday in my thesis progress.

Finally, I dedicate this thesis to my love Gizem without whom neither me nor my thesis would be meaningful.

ABSTRACT

AN INVESTIGATION OF SYSTEM IDENTIFICATION WITH ECCENTRIC MASS SHAKERS

This thesis deals with the problem of system identification of a structure tested with eccentric mass shakers. The analysis methods studied for this purpose are Eigensystem Realization Algorithm applied with Auto-Regressive Exogeneous models, Frequency Domain Decomposition technique and Covariance Driven Stochastic Subspace method. The Eigensystem Realization Algorithm is analyzed for the scenario when the input and the output data can be measured in eccentric mass shaker experiments. The Frequency Domain Decomposition is used for the experiments in which it is not possible to measure the phase angle between the input and the output. The Covariance Driven Stochastic Subspace method is another output-only identification scheme analyzed for making a sine-sweep experiment with eccentric mass shakers.

First, modal parameter identification capabilities of three methods are illustrated by a Monte Carlo analysis. Monte Carlo analysis is handled with the data simulated from a spring-dashpot model. Then a finite element model building is introduced and the building model is loaded in finite element analysis program to simulate a forced vibration test conducted with eccentric mass shakers. To apply the proposed methods, necessary modifications in testing an actual building are introduced. Finally, the results of the simulation of the experiments are introduced.

ÖZET

EGZANTRİK KÜTLELİ SARSMA CİHAZLARI KULLANARAK SİSTEM ÇÖZÜMLEME DENEYLERİNİN İNCELENMESİ

Bu çalışmada, dış merkezli kütleli sarsma cihazları test edilen yapıların çözümlenmesi problemi incelenmiştir. Yapının çözümlenmesi için kullanılan analiz metodları Oto-Regresif Dışsal modeller ile uygulanan Özdeğer Realizasyon Algoritması (Eigensystem Realization Algortihm), Frekans Düzlemi Ayrıştırması ve Ortak Değişintiler Tabanlı Altuzay Yöntemi'dir. İlk yöntem, sarsma deneylerinde girdi ve çıktıların ölçülebildiği durumların analizinde kullanılmıştır. İkinci yöntem, söz konusu deneylerde girdi ve çıktılar arasındaki faz farkının ölçülemediği durumlarda yapının çözümlenmesi için kullanılmıştır. Üçüncü yöntem ise frekans süpürme deneylerinde çözümleme yapmak için kullanılmıştır.

İlk olarak, yöntemlerin modal parametre bulgularının doğruluğu Monte Carlo analizi ile incelenmiştir. Monte Carlo simülasyonlarında yay-sönümleyici model kullanılmıştır. Daha sonra bir binanın sonlu elemanlar modeli hazırlanıp, sarsma deneylerinin simulasyonu yapılarak veri elde edilmiştir. Gerçek deney uygulamalarında önerilen metodların uygulanabilmesi için gerekli düzenlemelerden bahsedilmiştir. Son olarak deney simülasyonlarının sonuçları ve bu sonuçlara dayanarak yapılan çıkarımlarla çalışma tamamlanmaktadır.

TABLE OF CONTENTS

LIST OF FIGURES

LIST OF TABLES

1. INTRODUCTION

1.1. Problem Definition

Engineering problems are categorized according to the known and unknown parts of system equations. As illustrated in Figure 1, mathematical variables in an observed system are inputs, outputs and system parameters.

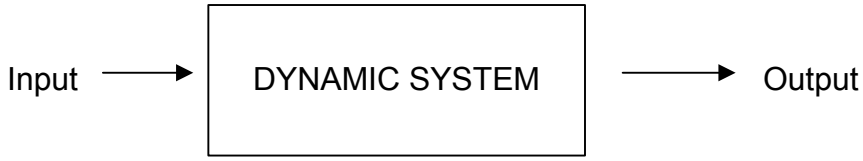

Figure 1.1. Illustration of a dynamic system

The most straightforward type of engineering problems are direct problems, which are defined as finding the response of a system to a known input when the system equations are also known. For example, with a given set of equations describing a space vehicle, the response of the vehicle to a given input can be found. The other types of engineering problems of dynamic systems are inverse problems. These types of problems are analyzed under the following three categories: (Bekey, 1970)

i. Given an input and output relationship, find a system description which fits such a physically realizable relationship as closely as possible. This is the design or synthesis problem which usually has additional constraints placed upon it. There is not a unique solution to the design problem, since infinitely large number of processes might have the same input-output relationship.
ii. Given a system description and response, find the input that caused it. This problem is known as the instrumentation problem. When the system equations are known and an input to generate a specified response is to be found, the problem is called the control problem in engineering.

iii. Given a set of input and corresponding outputs, find a mathematical model of the system. This problem, which is probably the most difficult inverse problem, is known as the system identification problem. For instance, finding properties of a reinforced concrete beam when applied input is known and output is measured is a system identification problem.

System identification can itself be separated into two categories according to the level of prior knowledge about the unknown system. If the mathematical laws and equations governing the system are totally "unknown", the problem is called the 'black-box' identification problem. Such problems are dealt with mathematical models that are suitable to generate same input-output maps with the analyzed systems, and they are mathematically simple. This notwithstanding, their variables do not give any explicit information about the nature of the system.

In the second type of the system identification problem, some knowledge about the nature of the problem is available, and such a problem is named 'grey-box' identification. In grey-box identification, a mathematical model that is related with the physical properties of the system is chosen and the problem is reduced to determination of the coefficients of the model. It is evident that most engineering modeling problems are the grey-box type, because usually enough knowledge exists concerning the basic equations of the system.

In general terms, an experimental system identification procedure is performed by exciting the system using some devices that induce a step, a sinusoid or a random signal as input to the system and observing input and output signals over a time interval. After performing the experiment, the first step is to choose an appropriate system identification method and to determine the unknown parameters of the mathematical model. The model obtained is tested to see whether it is an accurate model or not. If it is not, with the feedback of the model, the procedure is repeated until the best fitted model is found. The procedure is illustrated in Fig. 2 schematically.

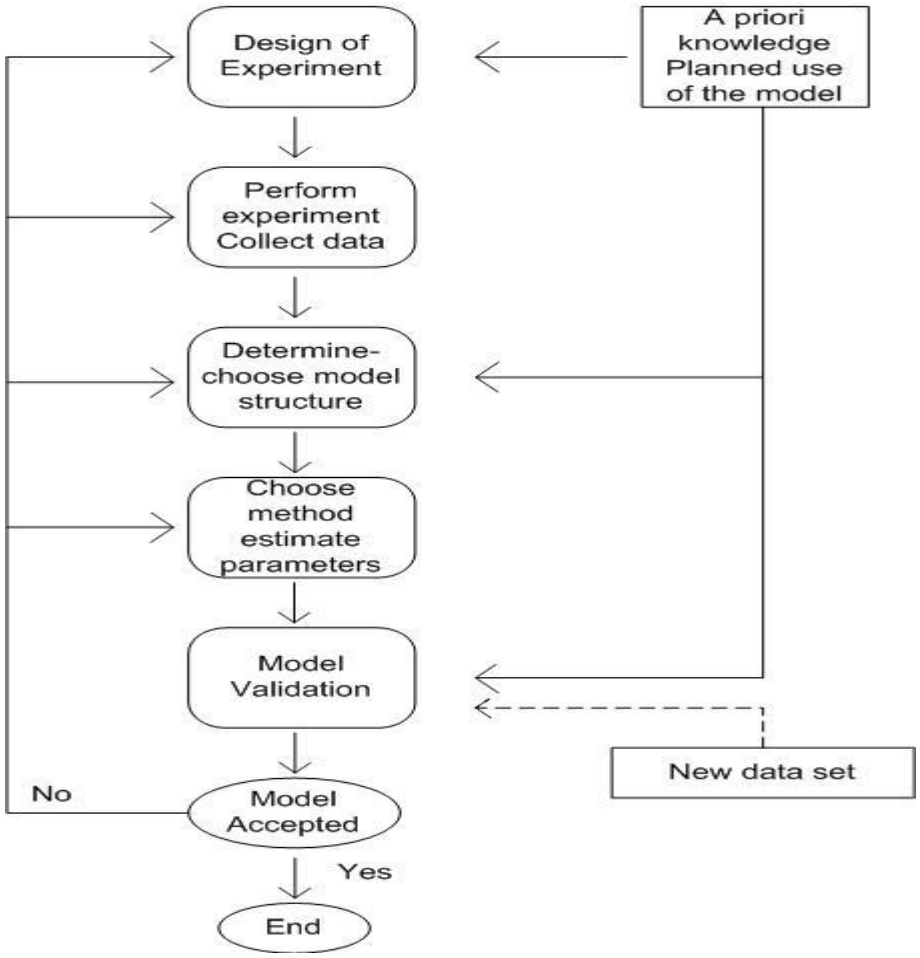

Figure 1.2. Schematic flowchart of system identification (Söderström and Stoica,1989)

Besides the theoretical challenges of the idealized system identification problem, experimental system identification copes also with the noise problem. In Fig.1.1, the problem is schematized ideally, but in real life applications there are two types of noises which are known as the process noise and the measurement noise. The process noise can be defined as the violation of the assumptions of physical modeling by the system itself because of the nature of the materials, manufacturing defects, etc. In the same manner, measurement noise is the error in observed data caused by electrical noise, imperfect calibration of devices and many other reasons for different disciplines.

The basic identification problem is a useful tool for different research areas such as economics, mechanical engineering, civil engineering, aerospace engineering, and so forth. Up until 1950s, much of system identification in engineering and control fields relied on Bode, Nyquist and Ziegler-Nichols charts, or on step response analysis. Though a lot of

results had already been developed in statistics and econometrics, two seminal papers published in 1965 paved the way to two main identification techniques that dominate the field today. The first one was the paper of Ho and Kalman that gave birth to the development of subspace identification and the second one was the paper of Aström and Bohlin that contributed to prediction error identification (Gevers, 2003).

Ho and Kalman (1965) provided a solution to state-space realization from impulse response data. The solution of this problem was later improved by Akaike (1974), which at the same time provided a solution to stochastic realization where a Markovian model can be obtained for a purely random system on the basis of covariance data. This method has evolved to subspace identification on early nineties.

The Astrom-Bohlin (1965) paper introduced the Maximum-Likelihood method that has been developed by time series analysts for the estimation of parameters of difference equations. In statistics, these methods are known as ARMA (Auto Regressive Moving Average) or ARMAX (Aute Regressive Moving Average with eXogeneous input). These models and the Maximum Likelihood models gave rise to the Prediction Error Method.

In the early nineties, a new epoch has started for system identification studies. In these years, researchers have found solutions to combine subspace identification and the stochastic realization theory. Larimore (1990), Van Overschee and de Moor (1994) and Viberg (1995) have provided solutions for Stochastic-Subspace Identification (SSI).

1.2. System Identification in Civil Engineering

The experimental study of structural vibration has always provided a major contribution to the efforts of understanding and controlling many vibration phenomena encountered in practice. Today, structural vibration problems present a major hazard and limitation for a wide range of engineering structures such as bridges, dams, off shore structures or wind turbines, for which structural integrity and thorough knowledge of dynamic characteristics of the structure is essential for design and maintenance purposes. The practice of system identification goes back to 1947, when Kennedy and Pancu have published a milestone paper in identification of natural frequencies and damping ratios of

civil structures with “resonance testing” (Ewins, 1984), and improvement of digital data processing and computer-assisted system identification methods have paved the way to online-health monitoring and model updating of civil structures.

Model updating and online-health monitoring are the fields of application of system identification in civil engineering. Finite element models are widely used in civil engineering for design purposes. It is a well-known fact that finite element models are always in conflict with dynamic test results. Model updating is the field that updates finite element models according to modal properties which are obtained with system identification experiments on the actual structure. Detailed survey of this subject can be found in Mottershed and Friswell (1993). Structural health monitoring (SHM) is described as “an active field of research, driven by the need to complement subjective visual inspection methods by objective nondestructive evaluation tools based on physical measurements and computer analyses” (Peeters, 2000).

SHM methods are divided into two categories: local and global SHM. Local SHM methods are the methods used by materials testing technologies, and global SHM techniques use system identification as its main tool. Vibration-based methods can be applied intermittently, implying a temporary deployment of the sensors and the acquisition system, or applied continuously, implying the embedment of the sensors in the structure. In the continuous setting, a shift from a preventive time-based to a predictive condition-based maintenance strategy is achieved. This shift reduces both the risk of a serious failure of the structure and the overall maintenance costs by excluding unnecessary inspection activities (Peeters, 2000). According to Rytter (1993), there are four levels of damage identification, which are detection, localization, assessment, and prediction.

System identification tests used in civil engineering can be classified as ambient vibration tests and forced vibration tests. Ambient vibration tests assume that the load induced to the structure by the wind, traffic, wave or any other external load source is a stationary random process and the tests are conducted by measuring the response of the structure in a specified time period. The conventional modal testing method is Peak Picking (PP) method which is basically based on curve fitting of frequency response functions (FRF) in frequency domain. Detailed investigation of the Peak Picking method

can be found in Ewins (1984) and Felber (1993). After the studies of Shih et al. (1988) and Brincker et al. (2000a), Peak Picking method has evolved to Frequency Domain Decomposition (FDD) method which is based on singular value decomposition of cross power spectrums of output signals and this method is subsequently enhanced in order to estimate damping ratios as Enhanced Frequency Domain Decomposition (Brincker et al., 2001).

Time domain parametric methods involve the choice of appropriate mathematical models to idealize dynamic structural behavior and the identification of modal parameters to minimize the error between the fitted and the actual models. These time domain methods are either applied with discrete time series or covariance functions. Ibrahim (1977) carries the ambient vibration analysis to time domain by applying random decrement technique to free vibration signals of a space craft. This method is known as Ibrahim Time Domain (ITD) technique or random decrement signature technique. James et al. (1993) make a new step in ambient vibration testing with Natural eXcitation Technique (NeXT) that calculates auto and cross correlations of output signal and uses this correlation function as representatives of impulse response functions in realization algorithms. The last step of ambient vibration analysis comes with Stochastic Subspace Slgorithms and is based on Akaike's 1974 paper that was improved by Van Overschee and De Moor (1993) as covariance driven stochastic subspace algorithms that uses output covariances in eigensystem realization and data driven stochastic subspace algorithms that uses output data projection.

Forced vibration testing of structures is based on applying a controlled force to a structure, measuring the applied force if necessary and possible, measuring the response of the structure and identifying system parameters according to the specified model. The forced vibration tests are applied by machines that induce load on the test structure by moving a mass while the machine is tied to the structure or by applying an impact by hitting the structure. Application of forced vibration tests relies on either estimation of frequency response functions or impulse response functions, that can be obtained through inverse Fourier transform of frequency response function.

The former methods of identification through forced vibration tests were developed in frequency domain. These were peak amplitude and circle-fit methods, which were based on curve fitting of frequency response functions of a single degree of freedom system, the details of which can be found in Ewins (1984). These methods can be applied with both forced vibration tests and ambient vibration tests, as mentioned above. A more sophisticated version of the peak picking method is the Rational Fraction Polynomial (RFP) method developed by Richardson and Formenti (1982). This method is the fitting of multi degree of freedom FRFs globally. Other frequency domain methods like the Complex Exponential Frequency Domain method and the Polyreference Frequency Domain method use nearly the same notion of curve fitting, and Allemang and Philips (1998) present the Matrix Polynomial Approach as a framework for unifying all these frequency domain methods.

Since there exist resolution and leakage problems in transferring data to frequency domain and then back to the time domain, direct time domain methods are also investigated and developed in the identification literature. Time domain methods in forced vibration testing are based on direct measurement of impulse response functions or estimation of impulse response functions with identification algorithms. Eigensystem Realization Algorithm (ERA), which is an extended version of Ho-Kalman algorithm, is developed by Juang and Pappa (1985) and is the most popular realization algorithm. Ibrahim Time Domain and Polyreference Complex Exponential algorithms are other time domain algorithms used along with forced vibration tests.

Forced vibration testing machines simply have masses that move, and apply force to test structure. Types of these machines are impact machines, sine-sweep machines, sine-step machines and pull-back machines.

Impact machines have a concentrated moving mass which accelerates along the stroke of the machine and contacts the test object for a brief moment. This sudden contact is representative of the Dirac delta function that produces the impulse response of the test structure.

Sine-sweep machines have a rotating mass that accelerates from an initial frequency to target frequency. In this acceleration period response of the structure over this period is measured, which contains the response of the system to all frequencies between initial and target frequencies.

Another kind of forced vibration testing is sine-stepping which is applied by eccentric mass shakers. Eccentric mass shakers are machines that apply sinusoidal force on structures by rotating masses in the machine. Typically, eccentric mass shakers have one or two rotating masses. When there are two masses, eccentricity of masses and their configuration can be arranged to apply various force configurations. In Figure 1.3, configuration of masses to apply forces in different directions can be seen.

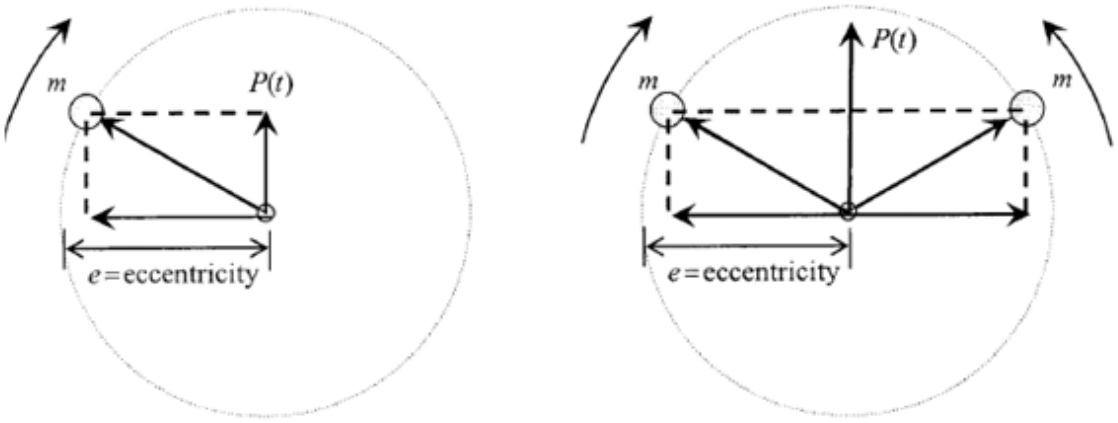

Figure 1.3. A schematic drawing of eccentric mass shakers (Felber,1993)

The amplitude of the force applied by an eccentric mass shaker depends on the frequency of rotating masses and on the eccentricity of the masses. The force applied is given by

$$P = m \times e \times \omega^2 \sin(\omega t) \tag{1.1}$$

where m is the mass, e is the eccentricity, and f the is frequency.

Testing procedure of sine-stepping involves starting at a frequency and applying a harmonic force to the structure until transient responses decay and only the steady-state response remains. After the steady-state response is reached the peak value is recorded, and the test continues to the next frequency step. Finally, a frequency response curve is

drawn and natural frequencies and damping ratios are identified from this curve as much as the frequency resolution allows. Mode shapes are identified by capturing the amplitude of frequency response function at each degree-of-freedom when the structure is excited at its natural frequency. Damping ratios are evaluated with the half-power bandwidth method.

The advantage of sine-sweep with eccentric mass shakers is having high signal to noise ratios. On the other hand, to obtain accurate results frequency increments should be as small as possible. Damping estimates with the half power bandwidth method do not give accurate results. The mode shape estimates are also erroneous, especially for high-rise buildings, because of the ripping effect, that is the phenomena that causes extra deflection in last stories.

Another problem of forced vibration tests is the testing time. Since eccentric mass shakers apply force with single frequency stepping, detailed investigation of crucial frequencies takes too much time. When damping ratio is low, the time necessary to wait for transient responses to die may take 2-3 minutes which might add up to hours when the whole frequency band is taken into consideration.

Identification of dynamic properties with sine-stepping is generally accomplished by curve fitting methods and frequency response function identification. Some other algorithms require white-noise input constraint on the data set. Theoretically, stationary white-noise signal is a signal containing sine waves with equal amplitudes at every point of the spectrum. Stationarity means having the same statistical property throughout time, and randomness requires infinitely many signals with different frequencies contributing in the white-noise signal.

Stochastic subspace methods and deterministic identification methods like ERA/OKID and N4SID require the input to the system be stationary white-noise. Because of this reason, when experiments are made with eccentric mass shakers, mostly curve-fitting methods are used to determine modal parameters. In this study, alternative ways of using eccentric mass shakers in system identification are investigated.

The first alternative way is to obtain white-noise-like data set by adding up all input and output signals recorded at each frequency during sine-step testing, so that the input-output data can be used to find an Auto Regressive eXogeneous (ARX) model of the system and impulse response sequence of this ARX model can be used in ERA to identify the system.

Second alternative analyzes the case when the input signal cannot be measured during the test. For this case, the FDD method is used for identification by adding up all output signals at all frequencies like the first case.

As the last alternative, it is investigated whether Covariance-driven Stochastic Subspace Identification method can be applied when transient responses are used. Normally steady-state responses are recorded in sine-step tests, but there are always transient responses when the mass starts to rotate to reach target frequency and when the mass accelerates from a frequency point to another.

This thesis is organized as follows. In Chapter 2, theoretical backgrounds of identification methods and how they can be modified to find a solution for the problem of system identification with eccentric mass shakers is introduced. In the Chapter 3, system identification of a two degree of freedom ideal spring-dashpot system is done with linear simulation data, and later the investigations are extended to the analysis of a more complex finite element model. In the fourth chapter applicability of these proposed methods to real life experiments is discussed and conclusions are proposed.

2. THEORETICAL BACKROUND OF IDENTIFICATION METHODS

2.1. Spatial Model

The continuous time equation of motion of a linear time-invariant system is given as:

$$\mathbf{M}\ddot{\mathbf{q}}(t)+\mathbf{L}\dot{\mathbf{q}}(t)+\mathbf{K}\mathbf{q}(t)=\mathbf{B}_f\mathbf{u}(t) \tag{2.1}$$

Equation (2.1) is a second order differential equation, in which $\mathbf{M}\in R^{N\times N}$, $\mathbf{L}\in R^{N\times N}$ and $\mathbf{K}\in R^{N\times N}$ are the mass, damping and stiffness matrices of the system, respectively, $\mathbf{q}(t)$, $\dot{\mathbf{q}}(t)$ and $\ddot{\mathbf{q}}(t)$ are the $N\times 1$ displacement, velocity and acceleration vectors and N is the number of degrees of freedom. $\mathbf{B}_f\in R^{N\times r}$ is the input influence matrix, indicating locations and possible scaling of input forces, $\mathbf{u}(t)$ is the non-zero forcing terms grouped together as an input vector, and r is the number of inputs. This equation represents the physical characteristics of a dynamic structural system and is referred to as the "spatial model".

The spatial model is built up on the assumption that the dynamic structure is a finite degree of freedom (DOF) system in which the masses are assumed to be concentrated at the DOFs. The second assumption is related with the damping properties of the system. Due to the lack of precise knowledge, the largest uncertainty is associated with damping and because of this uncertainty there are various kinds of damping models. In the linear viscous damping model, the damping forces are assumed to be proportional to the velocities, and the proportionality constants (called damping coefficients) are assumed to be constant. Third assumption is that the stiffness matrix is time invariant and constant, which is a well founded assumption as demonstrated by Trifunac (1972).

2.2. State-Space Models

So far, the equation of motion in second order linear differential equation form is introduced. An alternative is to express the equation of motion in first order differential equation form. Assuming that the matrix $\mathbf{M}$ is invertible, Equation (2.1) can be solved for $\ddot{\mathbf{q}}$ as,

$$\begin{aligned}\dot{\mathbf{q}}(t) &= \dot{\mathbf{q}}(t)\\ \ddot{\mathbf{q}}(t) &= -\mathbf{M}^{-1}\mathbf{L}\,\dot{\mathbf{q}}(t) - \mathbf{M}^{-1}\mathbf{K}\,\mathbf{q}(t) + \mathbf{M}^{-1}\mathbf{B}_\mathbf{f}\mathbf{u}(t)\end{aligned} \tag{2.2}$$

The equation in the first line is a simple equation that helps to express the second order equation in first order form. Now, the Equation (2.2) can be written in first order form as:

$$\frac{d}{dt}\begin{bmatrix}\mathbf{q}(t)\\ \dot{\mathbf{q}}(t)\end{bmatrix} = \begin{pmatrix}\mathbf{0} & \mathbf{I}\\ \mathbf{-M^{-1}K} & \mathbf{-M^{-1}L}\end{pmatrix}\begin{bmatrix}\mathbf{q}(t)\\ \dot{\mathbf{q}}(t)\end{bmatrix} + \begin{bmatrix}\mathbf{0}\\ \mathbf{M^{-1}B_f}\end{bmatrix}\mathbf{u}(t) \tag{2.3}$$

Then the state-vector is defined as:

$$\mathbf{x}(t) = \begin{bmatrix}\mathbf{q}(t)\\ \dot{\mathbf{q}}(t)\end{bmatrix} \tag{2.4}$$

and the system matrices are defined as:

$$\mathbf{A}_C = \begin{pmatrix}\mathbf{0} & \mathbf{I}\\ \mathbf{-M^{-1}K} & \mathbf{-M^{-1}L}\end{pmatrix} \quad \mathbf{B}_C = \begin{bmatrix}\mathbf{0}\\ \mathbf{M^{-1}B}_f\end{bmatrix} \tag{2.5}$$

Now, the state equation for a linear dynamic system can be written as:

$$\dot{\mathbf{x}}(t) = \mathbf{A}_c\,\mathbf{x}(t) + \mathbf{B}_c\mathbf{u}(t) \tag{2.6}$$

For an N DOF system the matrix $\mathbf{A}_c \in R^{2N\times 2N}$ is called the continuous time state transition matrix, $\mathbf{B}_C \in R^{2N\times r}$, where r is the number of input forces, is called the input matrix. Equation (2.6) is called the continuous time state-space model of the system.

In control and system identification problems, besides the equation of motion describing the dynamics of the system, there is another set of equations describing the output or measured quantities in terms of variables describing the dynamics of the system. This equation can be introduced as:

$$\mathbf{y}(t) = \mathbf{C}\,\mathbf{x}(t) \tag{2.7}$$

where $\mathbf{y}(t)$ is an $m\times 1$ vector where m is the number of the observed outputs, $\mathbf{C}$ is the output influence matrix which is an $m\times 2N$ matrix that shows the DOF the output measurement belongs to.

The output vector in Equation (2.7) is formulated so that it contains displacement and/or velocity measurements obtained at the DOF. In practice, acceleration measurements are also available, in which case the Equation (2.7) should be modified. As can be seen from Equation (2.2), accelerations are not only functions of the displacement vector but also the input force. When the outputs are accelerations, one has

$$\mathbf{y} = \mathbf{C}_a\,\ddot{\mathbf{q}} \tag{2.8}$$

where $\mathbf{C}_a \in R^{m\times N}$.

Substituting the second equation in Equation (2.2) for $\ddot{\mathbf{q}}$ into Equation (2.8) yields:

$$\mathbf{y} = \mathbf{C}_a\mathbf{M}^{-1}[\mathbf{B}_f\mathbf{u} - \mathbf{L}\,\dot{\mathbf{q}} - \mathbf{K}\,\mathbf{q}] \tag{2.9}$$

Then the general form of Equation (2.7) can be written as,

$$\mathbf{y} = \mathbf{C}\mathbf{x} + \mathbf{D}\mathbf{u} \tag{2.10}$$

where,

$$\mathbf{C} = [-\mathbf{C}_a\mathbf{M}^{-1}\mathbf{K} \quad -\mathbf{C}_a\mathbf{M}^{-1}\mathbf{L}] \qquad \mathbf{D} = \mathbf{C}_a\mathbf{M}^{-1}\mathbf{B}_f \tag{2.11}$$

The term $\mathbf{D} \in R^{m \times r}$, where m is the number of outputs and r is the number of input forces, is called the direct-transmission term. It directly transmits the input $\mathbf{u}$ to the output $\mathbf{y}$ without going through the intermediate state equation. The $\mathbf{D}$ matrix is a zero matrix when accelerations measurements are not contained in the output vector. The $\mathbf{D}$ matrix is set up by choosing appropriate rows of the matrix $[\mathbf{M}^{-1}\mathbf{B}_f]$ according to the DOF from which the output measurements are taken. Thus the complete state-space representation of an observed system can be given as,

$$\begin{aligned} \dot{\mathbf{x}}(t) &= \mathbf{A}_c\mathbf{x}(t) + \mathbf{B}_c\mathbf{u}(t) \\ \mathbf{y}(t) &= \mathbf{C}\mathbf{x}(t) + \mathbf{D}\mathbf{u}(t) \end{aligned} \tag{2.12}$$

The state-space model described hitherto is coordinate dependent. To prove this property, let the state vector $\mathbf{x}$ be transformed by a transformation matrix $\mathbf{T}$

$$\mathbf{z} = \mathbf{T}\mathbf{x} \tag{2.13}$$

Multiplying Equations (2.6) and (2.7) with $\mathbf{T}$, and replacing $\mathbf{x}$ with $\mathbf{T}^{-1}\mathbf{z}$ Equation (2.14) can be written as:

$$\begin{aligned} \dot{\mathbf{z}} &= \mathbf{T}\mathbf{A}_c\mathbf{T}^{-1}\mathbf{z} + \mathbf{T}\mathbf{B}_c\mathbf{u} \\ \mathbf{y} &= (\mathbf{C}\mathbf{T}^{-1})\mathbf{z} + \mathbf{D}\mathbf{u} \\ \bar{\mathbf{A}}_c &= \mathbf{T}\mathbf{A}\mathbf{T}^{-1} \quad \bar{\mathbf{B}}_c = \mathbf{T}\bar{\mathbf{B}}_c \quad \bar{\mathbf{C}} = \mathbf{C}\mathbf{T}^{-1} \end{aligned} \tag{2.14}$$

State-space matrices in new coordinates are $\bar{\mathbf{A}}_c, \bar{\mathbf{B}}_c$ and $\bar{\mathbf{C}}$. Direct transmission term $\mathbf{D}$ is coordinate independent. The new state-space matrices describe the same input-output mapping with a new state vector.

When the system represented by a state-space model is classically damped and the modes are underdamped, $\mathbf{A}_c$ has $\mathbf{N}$ complex conjugate pairs of poles and $\mathbf{N}$ complex conjugate pairs of eigenvectors. These poles can be expressed as:

$$\lambda_{2i-1}^c = \sigma_i^c + j\omega_i^c = (\lambda_{2i}^c)^* = \sigma_i^c - j\omega_i^c \tag{2.15}$$

and the frequencies and the damping ratios for the modes can be evaluated as:

$$\begin{aligned} \omega_i &= \sqrt{(\sigma_i^c)^2 + (\omega_i^c)^2} \\ \zeta_i &= \frac{-\sigma_i^c}{\omega_i^c} \end{aligned} \tag{2.16}$$

When the state-space model of a system is constructed, the response of the system to an input sequence can be found by:

$$\mathbf{x}(t) = e^{\mathbf{A}_c(t-t_0)}\,\mathbf{x}(t_0) + \int_{t_0}^{t} e^{\mathbf{A}_c(t-\tau)}\mathbf{B}_c\mathbf{u}(\tau)d\tau \tag{2.17}$$

Equation (2.12) is a continuous-time state-space representation of dynamic physical models, but system identification procedures and control systems work with digital computers and sensors that make calculations and sampling digitally. Thus, solutions to models should be discretized to be handled in digital computers. While transferring to discrete time, sampling interval, Δt is chosen and the value of discretized series are assumed to be constant, linearly varying or changing as a high order function throughout a sampling interval Δt. These assumptions are named zero order hold, first order hold or higher order holds. When a sampling point is represented as the k'th point, Equation (2.18) can be written as:

$$\mathbf{x}[(k+1)\Delta t] = e^{\mathbf{A}_c(k\Delta t)}\,\mathbf{x}(k\Delta t) + \int_{k\Delta t}^{(k+1)\Delta t} e^{\mathbf{A}_c((k+1)\Delta t-\tau)}\mathbf{B}_c\mathbf{u}(\tau)d\tau \tag{2.18}$$

After manipulating Equation (2.18) and evaluating the integral, discrete-time state-space model of a dynamic system can be obtained as,

$$\begin{aligned}
&\mathbf{x}(k+1) = \mathbf{A}_d\,\mathbf{x}(k) + \mathbf{B}_d\mathbf{u}(k) \\
&\mathbf{y}(k) = \mathbf{C}\,x(k) + \mathbf{D}\mathbf{u}(k) \\
&\mathbf{A}_d = e^{\mathbf{A}_c \Delta t} \\
&\mathbf{B}_d = \int_0^{\Delta t} e^{\mathbf{A}_c (k+1)\Delta t - \tau} \mathbf{B}_c\, d\tau
\end{aligned} \tag{2.19}$$

C and **D** matrices are same for continuous-time and discrete time state-space models because they are the matrices that only generate subspaces of vector $\mathbf{x}(t)$. Then, if initial state $\mathbf{x}(0)$, discrete-time model and input sequence are known for a system, response sequence of the system to the input can be found as:

$$\begin{aligned}
&\mathbf{x}(k) = \mathbf{A}_d{}^k\,\mathbf{x}(0) + \sum_{i=0}^{k-1} \mathbf{A}_d^i \mathbf{B}_d \mathbf{u}(k-i-1) \\
&\mathbf{y}(k) = \mathbf{C}\mathbf{A}_d{}^k\,\mathbf{x}(0) + \sum_{i=0}^{k-1} \mathbf{C}\mathbf{A}_d^i \mathbf{B}_d \mathbf{u}(k-i-1) + \mathbf{D}\mathbf{u}(k)
\end{aligned} \tag{2.20}$$

The sequence of matrices in generalized formula of finite difference representation of state-space model response, $\mathbf{D}, \mathbf{CB}, \mathbf{CAB}, \mathbf{CA^2B}, \mathbf{CA^3B}, \mathbf{CA^4B}, \mathbf{CA^5B}$... are called the weighting sequence or Markov parameters of the system. This sequence of matrices is the response of a dynamic system to a unit pulse applied at time step k when initial conditions are zero and all inputs are zero except the one at k'th time step, for single input case. When the system is a multiple input system, the columns of Markov parameters are the response of the system to a unit pulse applied at each DOF. First columns of Markov parameters are the response to a unit pulse applied at the first DOF, second columns of Markov parameters are the response of the system to a unit pulse applied at the second DOF and so on. It is worth mentioning that although system matrices $\mathbf{A}, \mathbf{B}$, and **C** are coordinate dependent, Markov parameters of a system are invariant under coordinate transformation.

2.3. Eigensystem Realization Algorithm

2.3.1. System Realization Theory

Many different system identification techniques in the field of structures have been developed. The process of constructing a state-space realization of a dynamic system from experimental data is called system realization. The time domain system realization methods in structural system identification are based on estimation of Markov parameters. System realization problem is to extract a state-space model of a system once Markov parameters of the system are known. The Markov parameters make it possible to construct a Hankel matrix as the basis for the realization of a discrete-time state space model of a system.

To construct a model, the first problem is to determine whether the system is controllable and observable. In following paragraphs, the concepts of observability and controllability are introduced.

A state $\mathbf{x}(k)$ is said to be controllable if that state can be reached from any initial state, with control actions, in a finite time interval (finite numbers of time steps in discrete time). To investigate this property, it is sufficient to determine whether all states can be reached from zero state conditions or not.

The theorem stating controllability conditions is as follows (Juang and Pappa,1985):

A linear, finite dimensional, discrete-time, constant dimensional system $\mathbf{x}(k+1) = \mathbf{A}\,\mathbf{x}(k) + \mathbf{B}\mathbf{u}(k)$ of order n is controllable if and only if the $n \times pr$ block controllability matrix $\mathbf{C}_p$ has rank n where

$$\mathbf{C}_p = \begin{bmatrix} \mathrm{B} & \mathrm{AB} & \dots & \mathrm{A}^{p-1}\mathrm{B} \end{bmatrix} \tag{2.21}$$

The other condition for minimal realization is observability. A state $\mathbf{x}(k)$ is said to be observable if knowledge of input $\mathbf{u}(k)$ and output $\mathbf{y}(k)$ over a finite time interval

completely determines $\mathbf{x}(k)$. If all states are observable the system is called completely observable or simply observable.

The theorem stating the observability condition is as follows (Juang and Pappa, 1985) :

The linear, finite dimensional, discrete time, constant dynamical system $\mathbf{x}(k+1) = \mathbf{A}\mathbf{x}(k) + \mathbf{B}\mathbf{u}(k)$ of order n with measurement equation $\mathbf{y}(k) = \mathbf{C}\mathbf{x}(k) + \mathbf{D}\mathbf{u}(k)$ of order m is observable if and only if the $mp \times n$ block observability matrix $\mathbf{O}_p$ has rank n where

$$\mathbf{O}_p = \begin{bmatrix} \mathbf{C} \\ \mathbf{CA} \\ \vdots \\ \mathbf{CA}^{p-1} \end{bmatrix} \tag{2.22}$$

A realization is the computation of system matrices $\mathbf{A}$, $\mathbf{B}$ and $\mathbf{C}$ from the Markov parameters identified with experimental data. Any system has an infinite number of realizations which have same input-output mapping for a given system. Minimum realization means the model with the smallest state-space dimensions among the systems realized that have the same input output mapping. All minimum realizations have the same set of eigenvalues, which are the modal parameters of the system (Juang Pappa,1985).

2.3.2. Application of the Eigensystem Realization Algorithm

Once Markov parameters of a system are known, there are several methods to compute the state-space representation of a system. Eigensystem Realization Algorithm (ERA) is one of the robust identification tools developed by Juang and Pappa (1985). To introduce ERA, let's denote the Markov parameters of a dynamic system as

$$\begin{aligned}
\mathbf{Y_0} &= \mathbf{D} \\
\mathbf{Y_1} &= \mathbf{CB} \\
\mathbf{Y}_2 &= \mathbf{CAB} \\
&\vdots \\
\mathbf{Y}_k &= \mathbf{CA}^{k-1}\mathbf{B}
\end{aligned} \tag{2.23}$$

The system realization starts with construction of $pm \times \gamma r$ Hankel matrix of order zero composed of Markov parameters:

$$\mathbf{H}(0) = \begin{bmatrix} \mathbf{Y_1} & \mathbf{Y_2} & \cdots & \mathbf{Y}_{\gamma} \\ \mathbf{Y_2} & \mathbf{Y}_3 & \cdots & \mathbf{Y}_{\gamma+1} \\ \vdots & \vdots & \vdots & \vdots \\ \mathbf{Y_p} & \mathbf{Y_{p+1}} & \cdots & \mathbf{Y_{p+\gamma-1}} \end{bmatrix} \tag{2.24}$$

Here p and γ are integers such that $\gamma r > pm$. It is worth noting that $\mathbf{D}$ is not included in Hankel matrix. Rank of the matrix $\mathbf{H}(0)$ is equal to system order n if $pm > n$ and $\gamma > n$. This point is more obvious when $\mathbf{H}(0)$ matrix is decomposed into two matrices as:

$$\mathbf{H}(0) = \mathbf{O}_p \mathbf{C}_{\gamma} \tag{2.25}$$

where $\mathbf{O}_p$ is the observability matrix given in Equation (2.22) and $\mathbf{C}_{\gamma}$ is the controllability matrix given in Equation (2.21). So if the order of the system is n, minimum dimensions of state matrix is $n \times n$, and if system is observable and controllable, the observability and the controllability matrices are of rank n. It becomes trivial to say that maximum order of the system that can be identified is pm.

ERA starts with the singular value decomposition of the $\mathbf{H}(0)$ matrix which can be expressed as:

$$\mathbf{H}(0) = \mathbf{USV}^T \tag{2.26}$$

where columns of matrices $\mathbf{U}$ and $\mathbf{V}$ are orthonormal, , and $\mathbf{S}$ is a diagonal matrix containing the singular values:

$$\mathbf{S} = \begin{pmatrix} \mathbf{S}_n & \mathbf{0} \\ \mathbf{0} & \mathbf{0} \end{pmatrix} \tag{2.27}$$

In Equation (2.27), $\mathbf{0}$'s are zero matrices with appropriate dimensions and $\mathbf{S}_n$ is a diagonal matrix with n non-increasing singular values in the diagonal.

Now, let $\mathbf{U}_n$ and $\mathbf{V}_n$ be matrices formed by first n columns of $\mathbf{U}$ and $\mathbf{S}$, respectively. Hence, $\mathbf{H}(0)$ is:

$$\mathbf{H}(0) = \mathbf{U}_n \mathbf{S}_n \mathbf{V}_n^T \tag{2.28}$$

In practice, the $\mathbf{0}$ matrices in $\mathbf{S}$ are never obtained as exact zeros because of numerical round off errors in computers, ill conditioning, noise and nonlinearities of the system. These are the main sources of error in system identification schemes. To deal with this problem, some algorithms like stability plots or cluster algorithms are applied to distinguish between system modes and noise modes.

From equations (2.28) and (2.25) , the following equality can be derived:

$$\mathbf{H}(0) = \left[\mathbf{U}_n \mathbf{S}_n^{1/2} \right] \left[\mathbf{S}_n^{1/2} \mathbf{V}_n^T \right] = \mathbf{O}_p \mathbf{C}_\gamma \tag{2.29}$$

From Equation (2.29) it can be concluded that when $\mathbf{O}_p$ and $\mathbf{C}_\gamma$ matrices are obtained, from definition of observability and controllability:

$\mathbf{B}$ = the first r columns of $\mathbf{C}_\gamma$

$\mathbf{C}$ =the first m rows of $\mathbf{O}_p$.

Up to this point of ERA, $\mathbf{B}$ and $\mathbf{C}$ matrices of a system are found. However, still the system matrix $\mathbf{A}$ is missing. To estimate the $\mathbf{A}$ matrix, first $\mathbf{H}(1)$ matrix should be formed as:

$$\mathbf{H}(1) = \begin{bmatrix} \mathbf{Y}_2 & \mathbf{Y}_3 & \cdots & \mathbf{Y}_{\gamma+1} \\ \mathbf{Y}_3 & \mathbf{Y}_4 & \cdots & \mathbf{Y}_{\gamma+2} \\ \vdots & \vdots & \vdots & \vdots \\ \mathbf{Y}_{p+1} & \mathbf{Y}_{p+2} & \cdots & \mathbf{Y}_{p+\gamma} \end{bmatrix} \tag{2.30}$$

Similar to Equation (2.29), following equation can be derived,

$$\begin{aligned} \mathbf{H}(1) &= \mathbf{O}_p \mathbf{A}^{\gamma} \\ \mathbf{H}(1) &= \left[\mathbf{U}_n \mathbf{S}_n^{1/2} \right] \mathbf{A} \left[\mathbf{S}_n^{1/2} \mathbf{V}_n^T \right] \end{aligned} \tag{2.31}$$

State matrix $\mathbf{A}$ can be solved from Equation 2.31 as:

$$\mathbf{A} = \mathbf{S}_n^{-1/2} \mathbf{U}_n^T \mathbf{H}(1) \mathbf{V}_n \mathbf{S}_n^{-1/2} \tag{2.32}$$

With the procedure hitherto described, $\mathbf{A}, \mathbf{B}$ and $\mathbf{C}$ matrices of a dynamic system can be obtained by constructing $\mathbf{H}(0)$ and $\mathbf{H}(1)$ matrices. The identified system matrices are not unique since the realized matrices are subject to coordinate transformation. Nevertheless, the state-space realization of $\mathbf{A}, \mathbf{B}, \mathbf{C}$ and $\mathbf{D}$ is a minimal realization and the identified system is observable and controllable.

2.3.3. Auto-Regressive Exogeneous Models

The auto-regressive exogenous models are used as mathematical representative of linear dynamic structural systems to obtain same input-output relationship with the observed model. The theoretical relationship between ARX models and linear dynamic models can be well understood by examining Unified Matrix Polynomial Approach. In the

study of Allemang and Phillips (1998), the matrix polynomials in frequency domain are investigated and shown to be valid for time domain.

In frequency domain, input-output relationship of a dynamic system is:

$$\mathbf{H}_{pq}(\omega_i) = \frac{\mathbf{X}_p(\omega_i)}{\mathbf{F}_q(\omega_i)} = \frac{\boldsymbol{\beta}_n(s_i)^n + \boldsymbol{\beta}_{n-1}(s_i)^{n-1} + ...\boldsymbol{\beta}_1(s_i)^1 + \boldsymbol{\beta}_0(s_i)^0}{\boldsymbol{\alpha}_d(s_i)^d + \boldsymbol{\alpha}_{d-1}(s_i)^{d-1} + ...\boldsymbol{\alpha}_1(s_i)^1 + \boldsymbol{\alpha}_0(s_i)^0} \tag{2.33}$$

Further rearranging this equation yields the following equation that is linear in the unknown α and β terms:

$$\sum_{k=0}^{d} \boldsymbol{\alpha}_k (s_i)^k \mathbf{X}_p(\omega_i) = \sum_{k=0}^{n} \boldsymbol{\beta}_k (s_i)^k \mathbf{F}_q(\omega_i) \tag{2.34}$$

$\boldsymbol{\alpha}_k$ and $\boldsymbol{\beta}_k$ are $m \times m$ and $m \times r$ coefficient matrices when the equations are developed from experimental data. When Equation (2.34) is post multiplied with $\mathbf{F}(\omega_i)^T$, where T is the complex conjugate transform operator, following relation can be obtained:

$$\mathbf{G}_{xf}(\omega_i) \sum_{k=0}^{d} [\boldsymbol{\alpha}_d (s_i)^k][\mathbf{G}_{xf}(\omega_i)] = \sum_{k=0}^{n} [\boldsymbol{\beta}_k (s_i)^k][\mathbf{G}_{ff}(\omega_i)] \tag{2.35}$$

In Equation (2.35), $\mathbf{G}_{xf}(\omega_i)$ and $\mathbf{G}_{ff}(\omega_i)$ are output-input cross spectra and input-input cross spectra, respectively. The previous cross spectra model can be reformulated to utilize FRF data by post multiplying both sides of equation by $[\mathbf{G}_{ff}(\omega_i)]^{-1}$

$$\sum_{k=0}^{d} [\boldsymbol{\alpha}_d (s_i)^k][\mathbf{G}_{xf}(\omega_i)][\mathbf{G}_{ff}(\omega_i)]^{-1} = \sum_{k=0}^{n} [\boldsymbol{\beta}_k (s_i)^k][\mathbf{G}_{ff}(\omega_i)][\mathbf{G}_{ff}(\omega_i)]^{-1} \tag{2.36}$$

Therefore the multiple input- multiple output FRF model is:

$$\sum_{k=0}^{d} [\boldsymbol{\alpha}_d (s_i)^k][\mathbf{H}(\omega_i)] = \sum_{k=0}^{n} [\boldsymbol{\beta}_k (s_i)^k] \tag{2.37}$$

The above model, in the frequency domain, is known as the ARX model as in the following formula:

$$\sum_{k=0}^{d} \boldsymbol{\alpha}_k \mathbf{y}(t_i + k) = \sum_{k=0}^{n} \boldsymbol{\beta}_k \mathbf{u}(t_i + k) \tag{2.38}$$

Since up to now it is shown that ARX models can be the mathematical counter-parts of linear dynamic models, we should now to introduce how to use ARX models along with ERA.

As stated in previous chapters, ERA uses impulse response functions to find state-space realizations of dynamic systems. There are several algorithms to find impulse response functions of a system. The impulse responses of a system can be directly measured by applying an impulse with a hammer or an impact machine, however this is not an easy and practical way, especially for actual structures because a weak impulse might not excite higher modes of the system and a strong impulse might cause local damage. Thus, generally impulse responses are found by first finding a mathematical model of the structure. Linear regressions are the simplest way of describing a parametric system, especially used in statistics. In the state-space and spatial models, system is described physically, however finite difference models are mathematical models just parametrizing systems with regression of time series. The corresponding model structure of finite difference models is:

$$\mathbf{y}(t) = \boldsymbol{\varphi}(t)\boldsymbol{\theta} \tag{2.39}$$

where $\mathbf{y}(t)$ is output, $\boldsymbol{\varphi}(t)$ is vector of regression variables comprising input and output and $\boldsymbol{\theta}$ contains the unknown model parameters.

ARX models are a type of finite difference models used to describe dynamic systems. ARX models given in Equation (2.38) can be written explicitly as:

$$\mathbf{y}(k) + \boldsymbol{\alpha}_1 \mathbf{y}(k-1) + ... \boldsymbol{\alpha}_p \mathbf{y}(k-p) = \boldsymbol{\beta}_0 \mathbf{u}(k) + \boldsymbol{\beta}_1 \mathbf{u}(k-1) + ... + \boldsymbol{\beta}_p \mathbf{u}(k-p) \tag{2.40}$$

where p is an integer indicating order of the model, $\mathbf{y}(k)$ is the output measured at time step k and $\mathbf{u}(k)$ is the input at time step k. The coefficient matrices $\boldsymbol{\alpha}_1, \boldsymbol{\alpha}_2 .... \boldsymbol{\alpha}_p$ of dimension $m \times m$ are associated with the $m \times 1$ output vectors $\mathbf{y}(k-1) .... \mathbf{y}(k-p)$, respectively and the coefficient matrices $\boldsymbol{\beta}_0, \boldsymbol{\beta}_1, ... \boldsymbol{\beta}_p$ of dimension $m \times r$ are associated with $r \times 1$ input vectors $\mathbf{u}(k), \mathbf{u}(k-1) .... \mathbf{u}(k-p)$ respectively. Equation (2.40) can be written in following form to obtain an equation in the form of Equation(2.39).

$$\mathbf{y}(k) = -\boldsymbol{\alpha}_1 \mathbf{y}(k-1) - .... - \boldsymbol{\alpha}_p \mathbf{y}(k-p) + \boldsymbol{\beta}_0 \mathbf{u}(k) + \boldsymbol{\beta}_1 \mathbf{u}(k-1) + ... + \boldsymbol{\beta}_p \mathbf{u}(k-p) \quad (2.41)$$

Equation (2.41) shows that output at time step k can be written in terms of p previous outputs and p previous inputs and the current input. This is the prediction of current measurement from previous data which is called forward-in-time prediction. Equation (2.41) can be written in vector form as follows;

$$\mathbf{y}(k) = \left[-\boldsymbol{\alpha}_1, -\boldsymbol{\alpha}_2, ..., -\boldsymbol{\alpha}_p, \boldsymbol{\beta}_0, \boldsymbol{\beta}_1, ... \boldsymbol{\beta}_p \right] \begin{bmatrix} \mathbf{y}(k-1) \\ \mathbf{y}(k-2) \\ . \\ . \\ . \\ \mathbf{y}(k-p) \\ \mathbf{u}(k) \\ \mathbf{u}(k-1) \\ . \\ . \\ . \\ \mathbf{u}(k-p) \end{bmatrix} \quad (2.42)$$

To be able to obtain a linear regression to find the coefficients of ARX model, Equation (2.42) can be written in matrix form by defining an output matrix as:

$$\mathbf{Y} = \left[\mathbf{y}(k), \mathbf{y}(k+1), ..., \mathbf{y}(k+l) \right] \tag{2.43}$$

and a coefficient matrix as:

$$\boldsymbol{\theta} = \left[-\boldsymbol{\alpha}_1, -\boldsymbol{\alpha}_2, ..., -\boldsymbol{\alpha}_{p,} \boldsymbol{\beta}_0, \boldsymbol{\beta}_1, ...\boldsymbol{\beta}_p \right] \tag{2.44}$$

and an input matrix as:

$$\boldsymbol{\Xi} = \begin{bmatrix} \mathbf{y}(k-1) & \mathbf{y}(k) & \cdots & \mathbf{y}(l) \\ \mathbf{y}(k-2) & \mathbf{y}(k-1) & \cdots & y(l-1) \\ \vdots & \vdots & \vdots & \vdots \\ \mathbf{y}(k-p) & \mathbf{y}(k-p-1) & \vdots & \mathbf{y}(k-p-2) \\ \mathbf{u}(k) & \mathbf{u}(k+1) & \cdots & \mathbf{u}(l) \\ \mathbf{u}(k-1) & \mathbf{u}(k) & \cdots & \mathbf{u}(l-1) \\ \mathbf{u}(k-2) & \mathbf{u}(k-1) & \cdots & \mathbf{u}(l-2) \\ \vdots & \vdots & \vdots & \vdots \\ \mathbf{u}(k-p) & \mathbf{u}(k-p+1) & \cdots & \mathbf{u}(l-p) \end{bmatrix} \tag{2.45}$$

Now the input-output relationship can be written as:

$$\mathbf{Y} = \boldsymbol{\theta}\boldsymbol{\Xi} \tag{2.46}$$

where $\mathbf{Y}$ is the $m \times ((l-k) \times m)$ output matrix, $\boldsymbol{\Xi}$ is the $((m+r+1) \times p) \times (l-k))$ input matrix containing both inputs and past outputs, and $\boldsymbol{\theta}$ is the $m \times ((r+1+m) \times p)$ unknown coefficient matrix. From Equation (2.46), if $(l-k) > p \times (m+r+1)$ and the input is rich enough to contain information about all modes of the system, a least squares solution can be found for the coefficient matrix $\boldsymbol{\theta}$ to represent the system mathematically.

Theoretically, ARX models can represent a linear dynamic system; however, in practice, output time history is a measured quantity which contains measurement noise and the system is not initially at rest because of the system noise. This problem causes errors in output prediction of ARX models. The estimated outputs approach true outputs when signal to noise ratio, the ratio of maximum amplitude of true outputs to maximum amplitude of noise, increases.

For an ARX model to be able to represent a multi input-multi output system , order of ARX model p should be sufficiently large so that $n \le p \times m$ where n is twice the number of degrees of freedom of the linear dynamic system and m is the number of observed outputs. To illustrate this clause, a 3-DOF spring-dashpot system is simulated by generating a white-noise input and calculating the response of the 3-DOF system is as output. Then, ARX models of the system are constructed for orders up to 20 and prediction error norms of ARX models are plotted versus ARX orders for various numbers of inputs and outputs. This plot is shown in Figure 2.1.

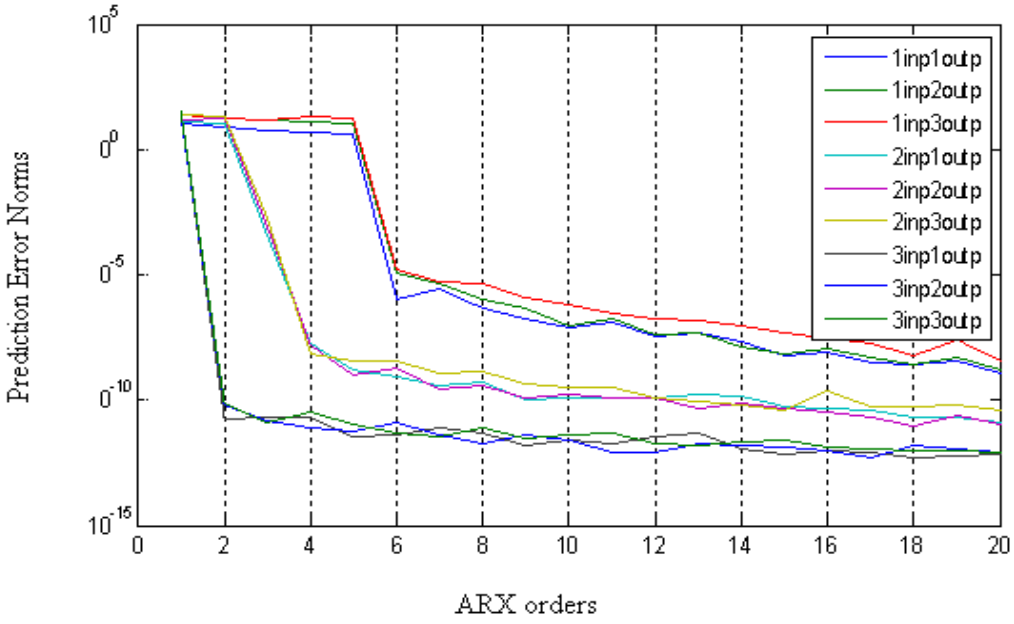

Figure 2.1. Prediction Error Norms vs. ARX orders

Figure 2.1and Figure 2.2, the ARX order should be higher than the order $p \times m$, after this point still the prediction order decreases but this decrease is to some extent. So for the sake of computational time, ARX order should be increased to some extent, but after some point is reached, increasing ARX order will only increase the computational time, and have no effect on prediction error.

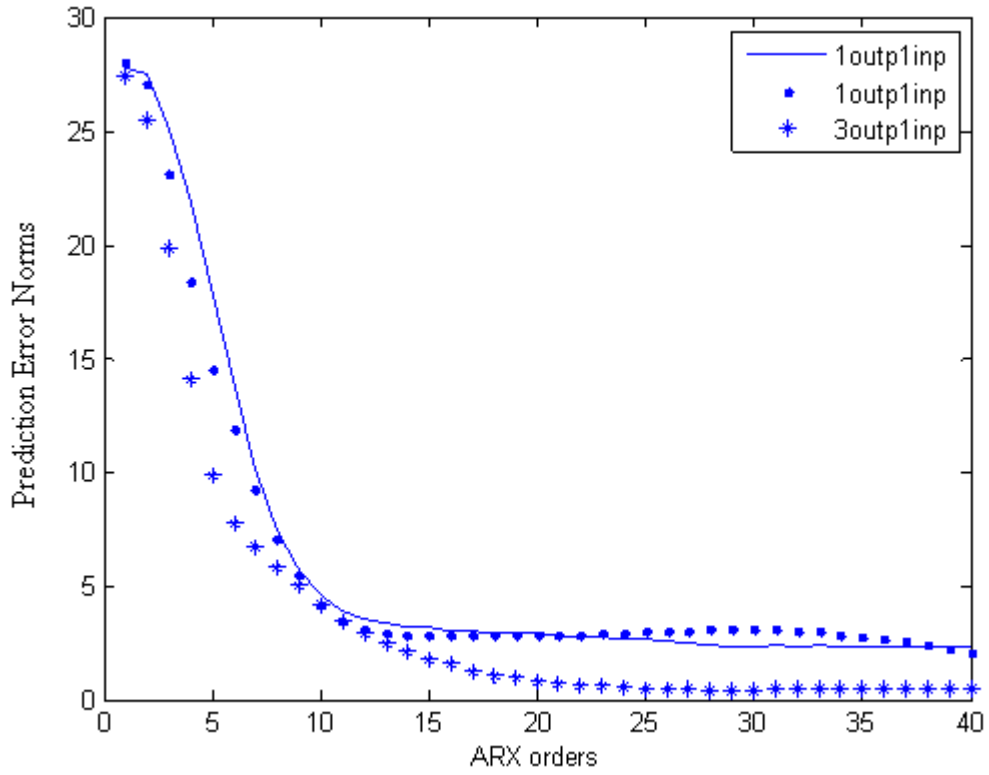

Figure 2.2. Prediction Error Norms vs. ARX orders for 5% noise

Up to this end, ARX models are introduced. The importance of ARX models is that, the pulse responses are estimated with ARX models to be used in ERA. Pulse response sequence of a system is output sequence of a system to a unit input applied at a time step when at previous and following time steps input is zero, and initial displacements are zeros in the system. So to observe pulse response sequence of a system, let the input vector be

$$\begin{bmatrix} u(k-p) \\ \vdots \\ u(k-1) \\ u(k) \\ u(k+1) \\ \vdots \\ u(k+s-1) \end{bmatrix} = \begin{bmatrix} 0 \\ \vdots \\ 0 \\ 1 \\ 0 \\ \vdots \\ 0 \end{bmatrix} \tag{2.47}$$

where dummy indices k and s are arbitrary integers, p is a number that must be larger than or equal to a specific number related to the order of the system and the number of outputs. The conditions at time k are called initial conditions and when system is initially at rest,

$$\begin{bmatrix} \mathbf{y}(k-p) \\ \vdots \\ \mathbf{y}(k-2) \\ \mathbf{y}(k-1) \\ \mathbf{y}(k) \end{bmatrix} = \begin{bmatrix} 0 \\ \vdots \\ 0 \\ 0 \\ 0 \end{bmatrix} \tag{2.48}$$

With these conditions the response of a single input-multi output (SIMO) system described by an ARX model as in Equation (2.42) will be:

$$\begin{bmatrix} \mathbf{y}(k) \\ \mathbf{y}(k+1) \\ \vdots \\ \mathbf{y}(k+1+s) \end{bmatrix} = \begin{bmatrix} \boldsymbol{\beta}_0{}^0 \\ \boldsymbol{\beta}_0{}^1 \\ \vdots \\ \boldsymbol{\beta}_0{}^{(s-1)} \end{bmatrix} \tag{2.49}$$

Equation (2.49) shows that the parameters $\boldsymbol{\beta}_0^0, \boldsymbol{\beta}_0^1, ..., \boldsymbol{\beta}_0^{(s-1)}$ form the pulse response sequence of a SIMO system. When the state equation, Equation (2.20), is solved for zero initial conditions and unit pulse in Equation (2.47), response of the system will yield:

$$\begin{aligned}
\mathbf{y}(k) &= \mathbf{D} \\
\mathbf{y}(k+1) &= \mathbf{CB} \\
\mathbf{y}(k+2) &= \mathbf{CAB} \\
&\vdots \\
\mathbf{y}(k+s-1) &= \mathbf{CA}^{s-2}\mathbf{B}
\end{aligned} \tag{2.50}$$

For the multiple input case, a unit pulse is applied to the system one at a time to obtain the corresponding column of Markov parameters. After applying a unit pulse at each degree of freedom one at a time, all columns of Markov parameters can be obtained and assembled to have system Markov parameters $\mathbf{D}, \mathbf{CB}, \mathbf{CAB}, \ldots \mathbf{CA}^{(s-2)}\mathbf{B}$. Dimension of each Markov parameter is $m \times r$ where m is the number of inputs and r is the number of outputs. So since equations (2.50) and (2.49) represent the pulse response sequence of the same system, Markov parameters can be obtained from the ARX model as;

$$\begin{aligned}
\boldsymbol{\beta}_0 &= \mathbf{D} \\
\boldsymbol{\beta}_0^{(1)} &= \mathbf{CB} \\
\boldsymbol{\beta}_0^{(2)} &= \mathbf{CAB} \\
\boldsymbol{\beta}_0^{(3)} &= \mathbf{CA}^2\mathbf{B} \\
&\vdots \\
\boldsymbol{\beta}_0^{(s-2)} &= \mathbf{CA}^{(s-2)}\mathbf{B}
\end{aligned} \tag{2.51}$$

To apply ERA for identification of a linear dynamic system, an ARX model is set up with an input-output data set, the Markov parameters of the system are estimated with the ARX model, and the Markov parameters are fed to ERA to extract modal parameters of the system.

2.4. Covariance Driven Stochastic Subspace Identification Technique

When introducing the stochastic realization problem, it is worth mentioning again that it was first developed by Akaike (1974). After Akaike's solution, James et al. (1993) provided the solution that cross-correlation functions are sums of decaying sinusoids of the

same form of the impulse response functions of a given system. The Covariance-Driven Stochastic Subspace (COV-SSI) method is based on these improvements and this evolution from deterministic to stochastic realization is robustly summarized by Alıcıoğlu (2006).

Recall that the state-space equations of a linear dynamic system are:

$$\begin{aligned} \mathbf{x}(k+1) &= \mathbf{A}\,\mathbf{x}(k) + \mathbf{B}\,\mathbf{u}(k) \\ \mathbf{y}(k) &= \mathbf{C}\,\mathbf{x}(k) + \mathbf{D}\,\mathbf{u}(k) \end{aligned} \tag{2.52}$$

where $\mathbf{x}(k) = \mathbf{x}(k\Delta t)$ is the discrete-time state vector, $\mathbf{A}$ is the discrete state matrix and $\mathbf{B}$ is the discrete input matrix. In practice there are always uncertainties including measurement and process noise. The process noise is due to disturbances and modeling inaccuracies, whereas measurement noise is due to sensor inaccuracies. Including these stochastic components, Equation (2.52) can be extended to consider process noise $\mathbf{w}_k$ and measurement noise $\mathbf{v}_k$, in the continuous-time stochastic state space model.

$$\begin{aligned} \mathbf{x}(k+1) &= \mathbf{A}\,\mathbf{x}(k) + \mathbf{B}\,\mathbf{u}(k) + \mathbf{w}_k \\ \mathbf{y}(k) &= \mathbf{C}\,\mathbf{x}(k) + \mathbf{D}\,\mathbf{u}(k) + \mathbf{v}_k \end{aligned} \tag{2.53}$$

In Equation (2.53) , process noise and measurement noise are assumed to be zero-mean white-noise and with covariance matrices,

$$E\begin{bmatrix} \mathbf{w}_p \\ \mathbf{v}_p \end{bmatrix}[\mathbf{w}_q^T \quad \mathbf{v}_q^T] = \begin{pmatrix} \hat{\mathbf{Q}} & \hat{\mathbf{S}} \\ \hat{\mathbf{S}}^T & \hat{\mathbf{R}} \end{pmatrix}\delta_{pq} \tag{2.54}$$

Where $E[\ ]$ is the expected value operator and δ_{pq} is the Kronecker delta. In stochastic processes like ambient vibration tests, $\mathbf{w}_k$ and $\mathbf{v}_k$ are assumed to be statistically independent of each other and the input sequence $\mathbf{u}(k)$ remains unmeasured and disappears from the Equation (2.53) (de Roeck et al., 2000). This results in the following discrete-time stochastic state-space model.

$$\begin{aligned}\mathbf{x}(k+1) &= \mathbf{A}\,x(k) + \mathbf{w}_k \\ \mathbf{y}(k) &= \mathbf{C}\,\mathbf{x}(k) + \mathbf{v}_k\end{aligned} \tag{2.55}$$

Another property of stochastic processes is that, the process $\mathbf{x}(k)$ itself is assumed to be zero mean and stationary like process noise and measurement noise:

$$E\left[\mathbf{x}(k)\right] = \mathbf{0}, E\left[\mathbf{x}(k)\mathbf{x}(k)^T\right] = \mathbf{\Sigma} \tag{2.56}$$

The term $\mathbf{\Sigma}$ in Equation (2.56) is defined as the state covariance matrix, and is independent of the time step k. This property is a result of the stationarity assumption that dictates the statistical properties of a random process to be invariant with respect to time. (Alicioglu 2006)

The output covariance matrices are defined as:

$$\mathbf{R}_i = E\left[\mathbf{y}(k+i)\mathbf{y}(k)^T\right] \tag{2.57}$$

and next state-output covariance matrix $\mathbf{G}$ is defined as

$$\mathbf{G} = E\left[\mathbf{x}(k+i)\mathbf{y}(k)^T\right] \tag{2.58}$$

After introducing these definitions following properties can be deduced;

$$\mathbf{\Sigma} = \mathbf{A}\mathbf{\Sigma}\mathbf{A}^T + \hat{\mathbf{Q}} \tag{2.59}$$

$$\mathbf{R}_0 = \mathbf{C}\mathbf{\Sigma}\mathbf{C}^T + \hat{\mathbf{R}} \tag{2.60}$$

$$\mathbf{G} = \mathbf{A}\mathbf{\Sigma}\mathbf{C}^{\mathbf{T}} + \hat{\mathbf{S}} \tag{2.61}$$

$$\mathbf{R}_i = \mathbf{C}\mathbf{A}^{i-1}\mathbf{G} \tag{2.62}$$

where $\hat{\mathbf{Q}}$, $\hat{\mathbf{R}}$ and $\hat{\mathbf{S}}$ are the covariance matrices of $\mathbf{w}_k$ and $\mathbf{v}_k$ given in Equation (2.54).

Equation (2.62) shows that output covariances can be considered as impulse responses of a deterministic, linear, time-invariant system. Therefore the classical realization theory can be applied to a stochastic system. This observation is used to feed classical algorithms like ERA with output covariances instead of impulse response functions.

The covariance matrices between outputs have already been defined in Equation (2.57). To start COV-SSI, the output covariances are gathered in a block Toeplitz matrix in which each diagonal consists of the repetition of the same element.

$$\mathbf{T}_i = \begin{bmatrix} \mathbf{R}_i & \mathbf{R}_{i\text{-}1} & \cdots & \mathbf{R}_1 \\ \mathbf{R}_{i+1} & \mathbf{R}_i & \cdots & \mathbf{R}_2 \\ \vdots & \vdots & \ddots & \vdots \\ \mathbf{R}_{2i\text{-}1} & \mathbf{R}_{2i\text{-}2} & \cdots & \mathbf{R}_i \end{bmatrix} \tag{2.63}$$

From the ergodicity assumption the covariances can be calculated using

$$\mathbf{R}_i = E\left[\mathbf{y}(k+i)\mathbf{y}(k)^T\right] = \lim_{l\to 0}\frac{1}{l}\sum_{k=0}^{l-1}\mathbf{y}(k+i)\mathbf{y}(k)^T \tag{2.64}$$

If a block Hankel matrix is defined as:

$$\mathbf{H} = \left[\begin{array}{cccc} \mathbf{y}(0) & \mathbf{y}(1) & \dots & \mathbf{y}(l-1) \\ \mathbf{y}(1) & \mathbf{y}(2) & \dots & \mathbf{y}(l) \\ \vdots & \vdots & \ddots & \vdots \\ \mathbf{y}(i-1) & \mathbf{y}(i) & \dots & \mathbf{y}(i+l-2) \\ \hline \mathbf{y}(i) & \mathbf{y}(i+1) & \dots & \mathbf{y}(i+l-1) \\ \mathbf{y}(i+1) & \mathbf{y}(i+2) & \dots & \mathbf{y}(i+l) \\ \vdots & \vdots & \ddots & \vdots \\ \mathbf{y}(2i-1) & \mathbf{y}(2i) & \dots & \mathbf{y}(2i+l-2) \end{array}\right] = \left[\begin{array}{c} \mathbf{Y}_p \\ \hline \mathbf{Y}_f \end{array}\right] \tag{2.65}$$

then, the Toeplitz matrix can be calculated using

$$\mathbf{T}_i = \frac{1}{l}\mathbf{Y}_f \mathbf{Y}_p^T \tag{2.66}$$

After obtaining the Toeplitz matrix, it can be decomposed as:

$$\mathbf{T}_i = \begin{bmatrix} \mathbf{C} \\ \mathbf{CA} \\ \vdots \\ \mathbf{CA}^{i-1} \end{bmatrix} \begin{bmatrix} \mathbf{A}^{i-1}\mathbf{G} & \mathbf{A}^{i-2}\mathbf{G} & \dots & \mathbf{G} \end{bmatrix} \tag{2.67}$$

Both the observability matrix and the reversed controllability matrix can be obtained by applying singular value decomposition (SVD) to the block Toeplitz matrix to get

$$\mathbf{T}_i = \mathbf{U}\mathbf{S}\mathbf{V}^T \tag{2.68}$$

where $\mathbf{U}$ and $\mathbf{V}$ are left and right singular vectors, and $\mathbf{S}$ is a diagonal matrix containing singular values in descending order.

With Equations (2.68) and (2.67) it can be stated that;

$$\begin{aligned} \mathbf{O}_i &= \mathbf{U}_1 \mathbf{S}_1^{1/2} \\ \mathbf{\Gamma}_i &= \mathbf{S}_1^{1/2} \mathbf{V}_1^T \end{aligned} \tag{2.69}$$

Since the inner dimension of the product $\mathbf{O}_i\mathbf{\Gamma}_i$ equals n and since we assume $n \le ri$, the rank of the product cannot exceed n.

As it was discussed before, zero matrices cannot be obtained very precisely in singular values matrix of Equation (2.68). If there is no measurement noise, the problem is simple since there exists a big gap between real singular values and the spurious ones, but when there is noise in the measured data, this gap disappears and some other algorithms are needed to differentiate between real modes and spurious modes.

Once $\mathbf{O}_i$ and $\mathbf{\Gamma}_i$ are known the solution to the system identification problem is straightforward. From Equation (2.67) it is known that $\mathbf{C}$ is equal to the first m rows of the O_i and the state-output covariance matrix $\mathbf{G}$ is the last m columns of $\mathbf{\Gamma_i}$. The state matrix A can be found by decomposing a shifted block Toeplitz matrix as:

$$\mathbf{T}_{i+1} = \mathbf{O}_i \mathbf{A} \mathbf{\Gamma}_i \tag{2.70}$$

and solving Equation (2.70) for $\mathbf{A}$, with Equation (2.69):

$$\mathbf{A} = \mathbf{O}_i^{\dagger} \mathbf{T}_{i+1} \mathbf{\Gamma}_i = \mathbf{S}_i^{-1/2} \mathbf{T}_{i+1} \mathbf{V}_1 \mathbf{S}_i^{-1/2} \tag{2.71}$$

where $(\bullet)^{\dagger}$ represents pseudo-inverse of a matrix. (Peeters and De Roeck, 1999)

At this point, system identification problem is solved theoretically with COV-SSI, and based on the output-covariances, $\mathbf{A}$, $\mathbf{G}$, and $\mathbf{C}$ are recovered. A first point worth to note here is that, when the COV-SSI is being applied, measurements are assumed to be infinite, whereas, in reality, measurements are not infinite and the covariance functions calculated by equation (2.66) are not the true covariance functions, but only estimates.

The COV-SSI introduced up to here is the Balanced Realization (BR) algorithm. In BR, principal components of the $\mathbf{T}_i$ matrix are used (Arun and Kung, 1990). Balanced state-space realization means that $\mathbf{O}_i$ and $\mathbf{\Gamma}_i$ matrices both have orthogonal columns and

$$\mathbf{O}_i^T \mathbf{O}_i = \mathbf{\Gamma}_i \mathbf{\Gamma}_i^T = \mathbf{S}_1 \tag{2.72}$$

There are some other realization algorithms in the literature. One of these algorithms is Canonical Variate Analysis (CVA) (Akaike,1975), which can be applied to COV-SSI method easily by defining weighing matrices to weight the $\mathbf{T}_i$ matrix as,

$$(\mathbf{T}_i)_W = \mathbf{W}_1 \mathbf{T}_i \mathbf{W}_2 \tag{2.73}$$

In CVA, the $\mathbf{T}_i$ matrix normalized by weighing to have singular values between 0 and 1. When CVA is applied, the singular values represent the cosines of the angles

between $\mathbf{Y}_p$ and $\mathbf{Y}_f$. The CVA improves the estimation results in COV-SSI by decreasing the effect of noise modes and amplifies those of the system modes (Guyader and Mevel, 2003). The weighting matrices are calculated as,

$$\mathbf{W}_1 = \left(\frac{1}{l} \mathbf{Y}_f \mathbf{Y}_f \right)^{-1/2} \qquad \mathbf{W}_2 = \left(\frac{1}{l} \mathbf{Y}_p \mathbf{Y}_p \right)^{-1/2} \tag{2.74}$$

When CVA is applied to COV-SSI method, only the Equation (2.69) should be modified as:

$$\begin{aligned} \mathbf{O}_i &= \mathbf{W}_1^{-1} \mathbf{U}_1 \mathbf{S}_1^{1/2} \\ \mathbf{\Gamma}_i &= \mathbf{S}_1^{1/2} \mathbf{V}_1^T \mathbf{W}_2^{-1} \end{aligned} \tag{2.75}$$

The rest of the COV-SSI method is same as the BR case of COV-SSI method. Throughout this study CVA is applied when COV-SSI method is used for system identification, because the BR and CVA realizations are compared and CVA is stated to give better estimates with COV-SSI method by Alıcıoğlu (2006).

2.5. Output Only Frequency Domain Decomposition

Output only frequency domain decomposition (FDD) is a combination of the peak picking method and the Complex Mode Indication Function (CMIF). In CMIF, frequency response function of a structure is identified when input is white noise and both input and output data are known. On the other hand the peak picking method consists of identification of structural properties by taking output data to frequency domain by discrete Fourier transform and conducting spectral analysis. Classical peak picking method is inaccurate especially when close modes are present and the CMIF method is inapplicable when input data set is not measurable. Frequency domain decomposition is superior in that sense to both CMIF and the peak picking method. In following section mathematical background of FDD is presented.

2.5.1. Complex Mode Indication Function and Frequency Domain Decomposition

Taking Laplace transform of Equation (2.1) leads to

$$\begin{aligned}\left[\mathbf{M}s^2+\mathbf{C}s+\mathbf{K}\right][\mathbf{q}]&=\left[\mathbf{B}_f\right]\mathbf{U}(s)\\ \left\{\mathbf{Y}(s)\right\}&=[\mathbf{C}]\mathbf{q}(s)\end{aligned} \tag{2.76}$$

This is the spatial model of a linear dynamic system in frequency domain. In the modal analysis area, the Equation (2.76) can be rewritten to express the relationship between input and output of a linear time invariant system as:

$$\mathbf{H}(i\omega)=\sum_{k=1}^{2N}\frac{\mathbf{A}_k}{i\omega-\lambda_k}=\sum_{k=1}^{2N}\frac{\mathbf{\Omega}_k\left\{\phi_k\right\}\left\{\Upsilon_k\right\}^T}{i\omega-\lambda_k} \tag{2.77}$$

Or in matrix form as:

$$\mathbf{H}(i\omega)=[\mathbf{\Phi}]\left[\frac{\mathbf{\Omega}_r}{i\omega-\lambda_r}\right][\Upsilon] \tag{2.78}$$

where N is the number of system modes, $\mathbf{H}\in R^{m\times r}$ is the FRF matrix, $\mathbf{A}_k$ is the k'th residue matrix of same size with FRF, $\left\{\phi_r\right\}$ is the $k'th$ mode vector of size $m\times 1$, $\left\{\Upsilon_k\right\}$ is the k'th modal participation vector of size $r\times 1$, $[\mathbf{\Phi}]\in R^{m\times 2N}$ is the mode shape matrix and $[\Upsilon]\in R^{r\times 2N}$ is the modal participation matrix.

In equations Equation (2.77) and Equation (2.78) the response of a structure due to a unit excitation force at a particular frequency is a linear combination of $2N$ residue matrices weighted by $(i\omega-\lambda_j)$.

The residue matrix is the product of the mode shape and modal participation matrices weighted by scaling factor $\mathbf{\Omega}_j$. Since the scaling of the mode shapes and the modal participation factors are arbitrary, the scaling factor obtained depends on the scaling of the

mode shape and the modal participation factor. If the mode shapes and modal participation factors can be scaled to be unitary, the scaling factor can be an indicator of the magnitude of the mode.

If SVD of the FRF is expressed as

$$[\mathbf{H}(i\omega)] = [\mathbf{U}(i\omega)][\mathbf{S}(i\omega)][\mathbf{V}(i\omega)]^T \tag{2.79}$$

it can be recognized that a similar form of Equation (2.78) is obtained.

If the number of dominant modes of structure is less than or equal to the smaller dimension of the FRF, left singular vectors are mode shapes and right singular vectors are modal participation factors. The singular values are then equivalent to scaling factors of each mode divided by the distance between sampling frequency and the pole location. For a given mode, when scaling factor is kept constant, the singular values obtained at SVD will increase at a spectral point close to a mode frequency. This is the indicator of a modal frequency in FDD. At the spectral lines around the modes, since the scaling factor of the closest mode shape becomes dominant, the first column of the left singular vectors is the mode shape vector of the system for the corresponding mode frequency (Shih et al., 1988).

The complex mode indication function (CMIF) is defined as the singular values of $[\mathbf{H}(i\omega)][\mathbf{H}(i\omega)]^T$. By this definition CMIF is square of the magnitude of the singular values of FRF (Shih et al., 1988).

In the CMIF method all singular values are plotted and in this plot the peaks of the highest singular values vector show mode frequencies. The peaks of other singular value vectors has peaks at dips of the highest singular value vectors which is caused by cross eigenvalue effect, which means thatthe secondary peaks occur where there is equal or close contribution of two modes. Thus when the second singular value is close to the first singular value in magnitude, it can be an indicator of a mode as well as the first singular value. The sources of error in this plot are the noise, the leakage effect of Fourier transformation and the nonlinearities of the dynamic structure.

CMIF method is applicable when FRF for broad-band frequencies can be determined with input-output data set. When only output can be measured, frequency domain decomposition technique which is mathematically similar with the CMIF technique is applied to identify system properties.

The relationship between the power spectral densities of inputs and outputs can be written as:

$$\mathbf{G}_{yy}(i\omega) = \mathbf{H}(i\omega)\mathbf{G}_{xx}(iw)\mathbf{H}(iw)^T \tag{2.80}$$

where $\mathbf{G}_{yy}(i\omega)$ is the power spectral density array of outputs; that is an array of values of auto-spectral densities and cross spectral densities which yields an $m \times m$ matrix at each frequency point and the (i, j)'th elements of these matrices are spectral density points of the i'th output with the j'th output. Power spectral density array of the inputs is obtained in the same way with $r \times r$ matrices at each frequency point.

For a white-noise input assumption, spectral density of the inputs is a matrix having same value at each element throughout all spectral lines. So spectral density matrix of a perfect white-noise can be assumed a constant value c. Imposing this assumption into Equation (2.80) the Equation (2.81) is obtained.

$$\begin{aligned}\mathbf{G}_{yy}(i\omega) &= [\mathbf{U}(i\omega)][\mathbf{S}(i\omega)][\mathbf{V}(i\omega)]^T c[\mathbf{V}(i\omega)][\mathbf{S}(i\omega)][\mathbf{U}(i\omega)]^T \\ \mathbf{G}_{yy}(i\omega) &= [\mathbf{U}(i\omega)]c[\mathbf{S}(i\omega)]^2[\mathbf{U}(i\omega)]^T\end{aligned} \tag{2.81}$$

Similarly, by substituting equation (2.79)into (2.80) leads to:

$$\begin{aligned}\mathbf{G}_{yy}(i\omega) &= [\mathbf{\Phi}][\frac{\mathbf{\Omega}_j}{i\omega - \lambda_j}][\mathbf{L}]c[\mathbf{L}]^T[\frac{\mathbf{\Omega}_j}{i\omega - \lambda_j}][\mathbf{\Phi}]^T \\ \mathbf{G}_{yy}(i\omega) &= [\mathbf{\Phi}]c[\frac{\mathbf{\Omega}_j}{i\omega - \lambda_j}]^2[\mathbf{\Phi}]^T\end{aligned} \tag{2.82}$$

Equation (2.81) shows that if the input is a white-noise, singular values of the power spectral density matrix of outputs will have a form similar to the singular values of the frequency response function if the singular value decomposition is scaled to have unitary singular vectors, except the fact that singular values at each frequency point will be amplified with spectral density of input, c. Thus, singular value decomposition of output spectral density matrix will have peaks at the mode frequencies for the highest singular value vector and the first column of the left singular matrix, corresponding to this peak will give mode shape vector of system.

In some cases, two modes dominate around a peak of singular values of the spectrum. In such cases, the first singular vector is a good estimate of the strong mode that means having higher mode participation value, if there is no or low mode coupling in the system, the second singular vector will be a good estimate of second mode. However, when there is mode coupling, bias on estimate of stronger mode shape will be small but bias on the estimate of weak mode will be strong. In this case it might be possible to estimate both of the mode shapes at different spectral lines, one line at which strong mode is dominant and another line at which weak mode is dominant (Brincker et al.,2000a).

In the case that the input force is a sinusoidal plus white-noise, if frequency of the harmonics in the input is known or an initial guess can be done, frequency domain decomposition can still be applied to find the mode shapes and frequencies. In this case value of the highest singular value of power spectral density will be enormously high around frequency of input when compared to other frequency points. However, still power spectral density of input is constant at frequencies far from input frequency. So the scaling factor in Equation (2.78) is constant for a given mode, and when the frequency point is close to the pole of the system, the singular values of the power spectral density matrix will be an indicator of a mode frequency and mode shape (Brincker et al., 2000b).

Frequency domain decomposition technique decomposes the system into a set of single degree of freedom systems, thus making it possible to identify damping ratios by finding the free decay functions of each single degree of freedom set. To find free decay functions first, the mode shape vectors at each peak are found. Then the mode shape vectors at each peak are compared with the left singular vectors at each spectral line

according to Modal Amplitude Coherence (MAC) criteria. MAC is stated by Juang (1994) as follows:

$$MAC_i = \left|\bar{\phi}_i \hat{\phi}_i^*\right| / \left(\left|\bar{\phi}_i \bar{\phi}_i^*\right| \left|\hat{\phi}_i \hat{\phi}_i^*\right|\right)^{1/2} \tag{2.83}$$

where $\bar{\phi}_i$ is the mode vector of peak, and $\hat{\phi}_i$ is the mode vector of a frequency point around the peak.

A SDOF spectral density function is determined by setting a minimum limit for the MAC and calculating MAC of the mode shape vector of the chosen peak with the singular vectors of spectral points around the peak. When MAC between the mode shape vector and a first singular vector of a spectral line is higher than the limit, the first singular value of this spectral line belongs to the SDOF power spectral density function of the given mode. This is done at all spectral points. By doing this, SDOF power spectral density function is found partially and the inverse Fourier transform of SDOF spectral density function is the free decay, auto correlation, function of the given mode. Then, all extremes of the free decay function is found as r_k , and since the logarithmic decrement of a free decay function is given as

$$\delta = \frac{2}{k} \ln\left(\frac{r_0}{|r_k|}\right) \tag{2.84}$$

where k is time step, r_0 is the initial value of the free decay function, and δ is the logarithmic decrement, the damping ratio is estimated with the following formula:

$$\zeta = \frac{\delta}{(\delta^2 + 4\pi^2)^{1/2}} \tag{2.85}$$

Equation (2.84), can be also written as:

$$2\ln(r_0) - k\delta/2 = 2\ln(|r_k|) \tag{2.86}$$

So if $2\ln(|r_k|)$ is regressed on k, the slope of the regressed function is the logarithmic decrement and damping can be found by Equation (2.86). However, the SDOF spectra can be only partially determined because of leakage and noise errors, thus the damping estimate is biased, as it would be also with the half-band width estimation of (Brincker et al., 2000).

3. SYSTEM IDENTIFICATION WITH COMPUTER SIMULATIONS

3.1. Spring-Dashpot System Example

To thoroughly illustrate the procedures for the three system identification methods introduced up to now, identification of a 2-DOF spring-dashpot model is simulated. The mass, stiffness and damping matrices of the 2-DOF model are given in Table 3.1.

Table 3.1. Mass, stiffness and damping matrices for the 2-DOF spring-dashpot model

Mass		Stiffness		Damping	
1	0	700	-200	1.35	-1.50
0	1	-200	500	-1.50	2.70

In the ERA and the COV-SSI methods, a state-space model is found from the measured data set. Once a state-space model is estimated, modal parameters are extracted from state-space matrices. The identification of a state-space model requires the definition of the model order of the real structure. To predict the model order is not straightforward, since there is noise in data in real life applications. The most appropriate way of determining the real model order is to identify state-space models within a pre-specified conservative interval, which means setting the upper limit to a much higher number than the predicted actual model order of the real system. The use of a high model order leads to the introduction of noise and spurious modes which have little to none physical relevance but are needed to model the noise.

The separation of physical modes from noise modes is a crucial step of ERA and COV-SSI algorithms. The most popular and simple way of achieving this is the creation of stabilization diagrams. In these diagrams, the modal parameters of estimated models are presented according to some preset stability criteria, or natural frequencies are plotted the

versus model order. The modes that appear in most of the models with consistent frequency, damping and mode shape values are considered stable, and are most likely to be physical modes.

Some modes that exist in most of the model orders are spurious modes. This situation makes it harder to distinguish physical modes from spurious modes without imposing some selection criteria to stabilization diagrams. Thus, classification of a mode as stable should be restricted by the defining some limits that check the variation of modal parameters from one model order to another, rather than including all the estimated modes in stabilization diagrams, In Figure 3.1, a stabilization diagram set up for the 2-DOF spring-dashpot system obtained with ERA is illustrated as an example.

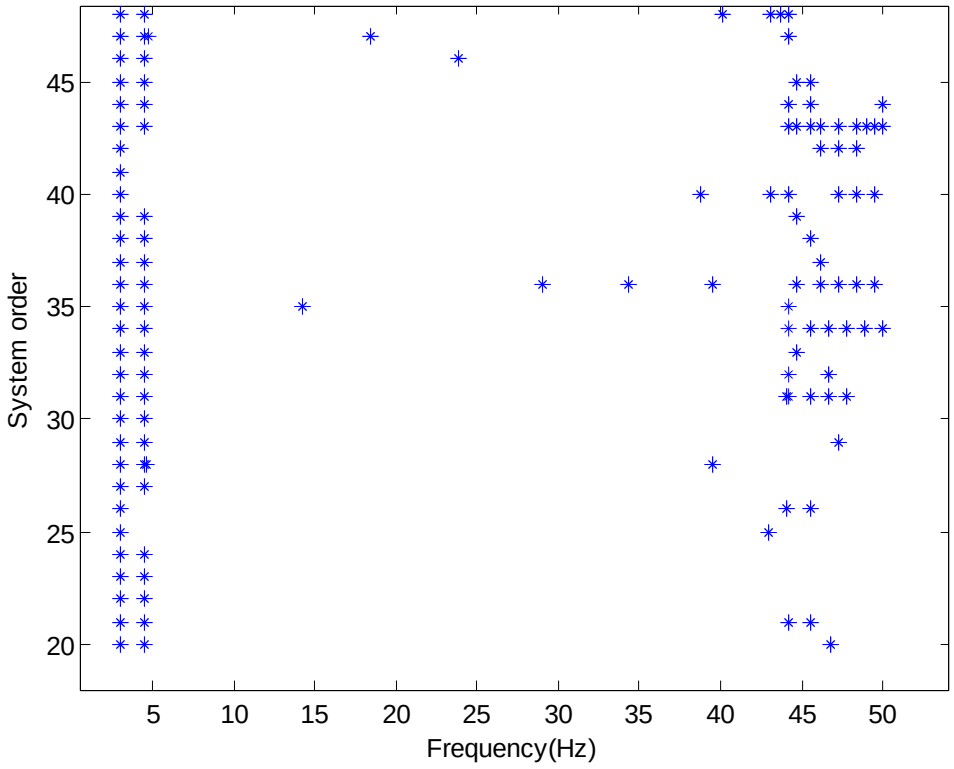

Figure 3.1. Stabilization diagram for the 2-DOF system

When a stabilization diagram is being constructed, first the highest model order is chosen and modal parameters for this model order are found. Then by gradually reducing the model order and finding the modal parameters, the lately found modal parameters are

compared with the modal parameters of previous model. The stability criteria for a mode are given by following formulas (Magalhaes et al.,2007):

$$\frac{\omega_p - \omega_{p+1}}{\omega_p} \le \rho_\omega \quad , \quad \frac{\zeta_p - \zeta_{p+1}}{\zeta_p} \le \rho_\zeta \quad , \quad 1 - MAC(\psi_p, \psi_{p+1}) \le \rho_{MAC} \tag{3.1}$$

where p is the model order, ω_p, ζ_p and ψ_p are frequency, damping and mode vector estimates at this order, and ρ_ω, ρ_ζ and ρ_{MAC} are user defined stability criteria. The MAC coefficient, which is a measure for checking how alike the estimated mode vectors are, was introduced previously in Chapter 2. For the stabilization diagram given in Figure 3.1, ρ_ω, ρ_ζ and ρ_{MAC} are 0.2 %, 0.5 % and 0.99 %, respectively. These parameters are chosen heuristically. To obtain clearer stabilization diagrams during identification procedure, a trial and error approach is the best way to determine the best stabilization criteria. If the parameters are chosen very strictly, weak modes might be considered unstable noise modes; on the other hand, if the stability parameters are loose, than some mathematical modes might become stable like physical modes. Power spectral density functions (PSD) are used along with stabilization diagrams to improve the physical mode selection procedure. PSD of each output channel is calculated, normalized and averaged, then the averaged normalized power spectral density (ANPSD) function of outputs is plotted onto stabilization diagrams. It is well known that output spectrums have peaks at the mode frequencies. Thus, plotting ANPSD onto the stabilization diagrams helps the user in visual inspection of mode frequencies.

Although stabilization diagrams are simple and effective tools in system identification for distinguishing physical modes, to have stabilization diagrams with good quality-that means clearer alignments of physical poles- and to choose the right physical poles, experienced users are needed. Along with the user's experience, the identification algorithm used, signal to noise ratio of the time series under analysis and characteristics of the structure are the major factors affecting the quality of the stabilization diagrams, and thus the accuracy of the identification results.

In the case of COV-SSI method, the number of block rows of the Toeplitz matrix used in the identification has strong influence on the quality of subsequent stabilization diagrams. If the lag of covariance functions calculated in COV-SSI is said to be p and m is the number of measured data channels, $p \times m \times \Delta t$ is the length of data in seconds which is the upper limit of mode periods that can be identified. As a consequence, during the configuration of a system identification program, it is essential to spend some time with the tuning of identification algorithm parameters.

Another point is that, for ERA, column to row ratio is an important factor affecting the quality of the results obtained. According to experiences reported in the literature, the best results are obtained with a column to row ratio of Hankel matrix between 2 and 4 (Juang, 1994). The size of the Hankel matrix is another parameter to be tuned by trial and error to improve identification results and decrease computational time.

As discussed up to now, stabilization diagrams are simple useful tools in system identification. However, the stabilization diagram itself does not solve the modal parameter identification problem in system identification, it is just a graphical tool to help with the manual selection of the modes that are more likely to be physical modes. In the context of continuous monitoring or automated identification, it is crucial to develop tools to select the physical modes without any user interaction.

With the inspection of clustering algorithms studied before (Scionti and Lanslots, 2005; Lau et al., 2007), a simple clustering algorithm is used in this study. In this algorithm first the stable poles identified with the stability criteria are stored, than these stable frequencies, damping ratios and mode shapes are clustered according to clustering criteria, defined similarly with stability criteria. After clustering the stable poles, largest groups of the poles are chosen as system poles. The number of poles to be chosen is to be set by the user.

The cluster algorithm mentioned is used in conducting a Monte Carlo analysis for ERA and COV-SSI algorithms. The Monte Carlo analysis consists of the following steps: First, a white-noise input is generated and applied to the linear dynamic system to be analyzed. Then, the simulated outputs are corrupted by adding white-noise series that have

standard deviations which are 5% of the standard deviations of the corresponding simulated outputs. These noisy outputs are used in the system identification algorithms. If the number of these simulations is sufficiently large, the distributions of parameter estimation errors are expected to be zero mean Gaussian. If this is not the case, it can be concluded that the results of the method is biased, and high bias causes mis-identification of the linear dynamic system with the analyzed identification method (Peeters, 2000).

To analyze the bias in ERA, the 2-DOF spring-dashpot system is simulated . During the simulations an input sequence with 100,000 data points is generated with 0.001 sampling time, the output data is resampled with 0.01 sampling time and filtered with a 50'th order Chebyshev filter, a 100 by 200 Hankel matrix is created and ERA with ARX is applied. Stabilization diagrams between 80 to 20'th order models are created and stable poles are clustered, and the simulations are repeated 200 times.

Figure 3.2 illustrates the observed frequency and damping ratio histograms of the identified natural frequencies and damping ratios obtained in the 200 runs. The ordinates in the histograms represent the number of simulations and the abscissa represents the ratio of estimated frequency to the actual frequency.

The results in Figure 3.2 show that the estimated parameters are distributed like normal distribution. Since deterministic ERA is used, the bias in identified frequencies is small. The ratio of identified frequencies to the actual frequencies fall within the ±0.001% range and the average of the ratio is close to 1. The ratio of identified damping ratios to the actual damping ratios fall into the ±0.01% range, but still the distribution is similar to normal distribution with average 1. The damping estimates have much higher bias compared with the frequency estimates, as expected.

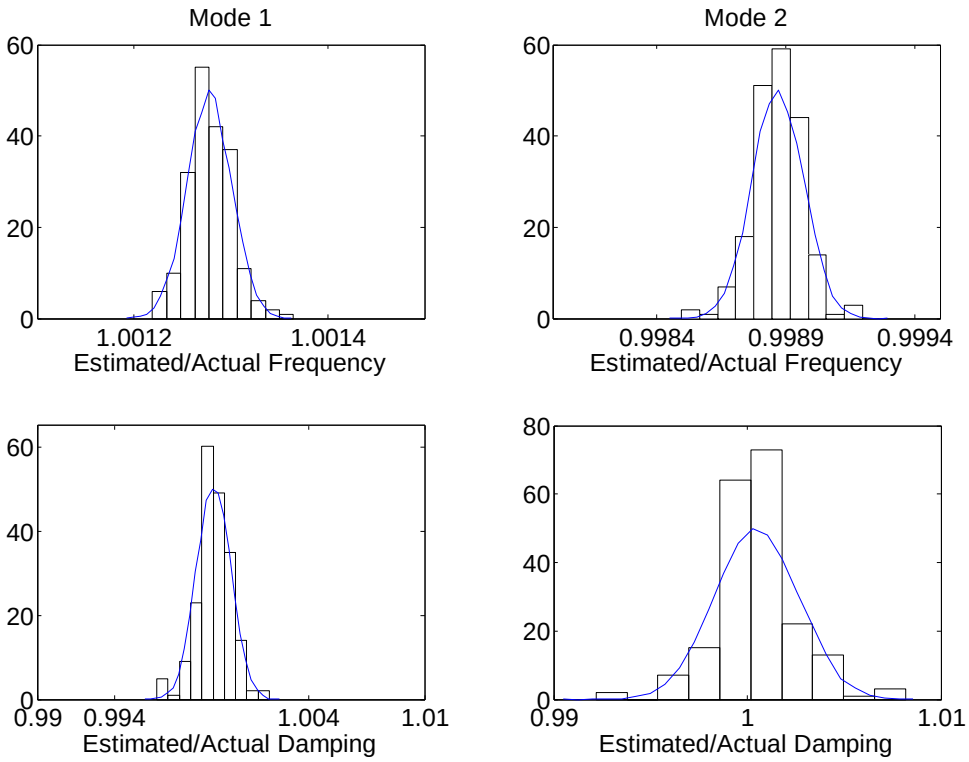

Figure 3.2. Observed frequency histograms for the natural frequencies and damping ratios estimated with ARX/ERA for 200 runs

To analyze the bias in the COV-SSI method, the same 2-DOF freedom system is used and the data is generated exactly as for the ERA/ARX case. 150 lag covariance functions of the output data are calculated, thus the covariance length is 3 seconds and a 300 by 300 Toeplitz matrix is created to apply the COV-SSI method. Models from 80 to 20'th orders are estimated to obtain the stabilization diagrams, and the stable poles are clustered to choose the system modes.

In Figure 3.3, the observed frequency and damping ratios are interpreted in histograms. It can be seen that the distribution of estimated parameters are similar to a normal distribution with mean close to 1, the estimated frequencies are distributed in a $\pm 2\%$ range, and the estimated damping ratios are distributed in a $\pm 50\%$ range. The bias associated with damping ratios is higher when compared with the frequency estimates.

The histograms indicate that both COV-SSI and ERA have low bias, thus it can be said that there is not a systematical error in either of the methods. The bias in the damping ratio estimates is higher, especially in COV-SSI. This is an expected result, because damping estimates depend on the phase difference and most of the information about phase angle is missing in output only methods. The estimated parameters are distributed in smaller intervals, especially for frequency estimates, in ERA.

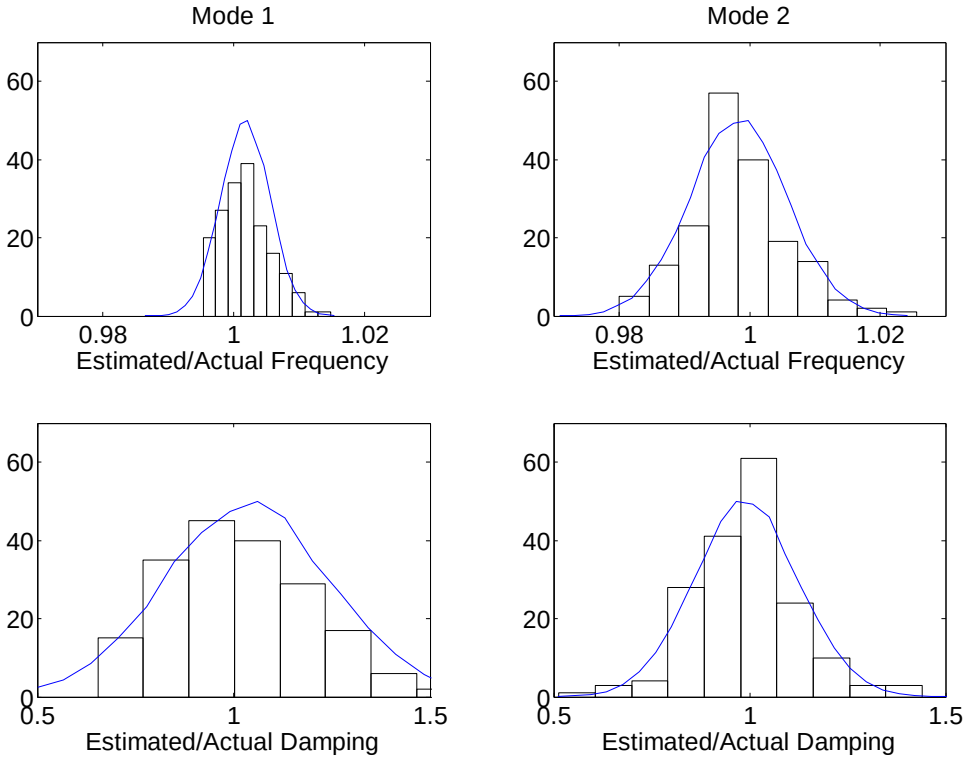

Figure 3.3. Observed frequency histograms for the natural frequency and damping ratios estimated with COV-SSI for 200 runs

For the last case, system identification of the FDD method is applied to the 2-DOF spring-dashpot system. Automatically selecting the physical modes is not applicable to the FDD method. Like the peak picking method, the physical modes are selected with visual inspection of a semi-log plot of the singular values of the power spectral density matrix. Thus Monte Carlo analysis is not applicable to the FDD method but to be able to make a comparison, system identification of the same spring-dashpot system is done for one simulation.

To simulate system identification of 2-DOF spring-dashpot system, a 200,000 point white-noise data series is created with 0.001 sampling time and output data is obtained with linear simulation of the 2-DOF spring dashpot system.

The estimate of the power spectral density (PSD) functions affects the accuracy of the FDD method. Throughout this study, the PSD functions of output data are calculated with Welch's method, which is a good method to estimate PSD functions. To increase the accuracy of spectrum estimation, and increase the calculation speed, Welch proposes to construct periodogram with the data and weight the data with windowing functions (Cooley et al., 1969). PSD functions of the output data are calculated with periodical Hanning window and the 10 data segments are assembled and averaged for each output data, and assembled into a PSD matrix in FDD.

The peaks of the singular value plot of the PSD matrix are interpreted as natural frequency points of the system and left singular vectors belonging to these singular values are the mode vectors of the system. As can be seen in Figure 3.4, the peaks of the highest singular values are around the natural frequencies of the system.

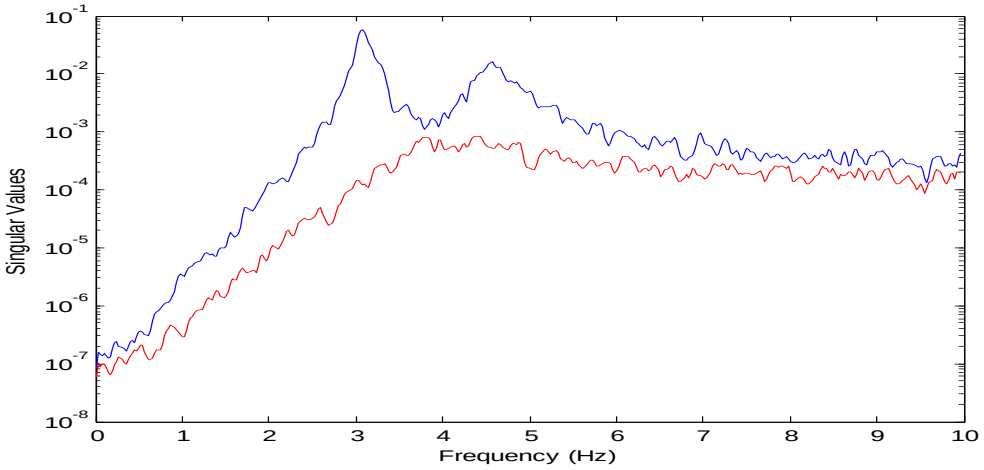

Figure 3.4 Singular Values of PSD matrix for 2-DOF system

In Figure 3.5 and Figure 3.6 the peaks are zoomed and mode frequencies are chosen for the system. Since the damping estimation is highly biased with the FDD method, and since for the forced vibration test case, damping estimation with FDD is impossible

because only the steady state part of data is recorded, damping estimation results are not interpreted.

The quality of results in the FDD method depends on the frequency resolution, which is 0.025 in this particular example. There is a tradeoff between the frequency resolution and the accuracy of the PSD estimate in Welch's method, because to have better frequency resolution, the data length of each periodogram should be increased, and increasing the data length of each periodogram results in less periodograms calculated and averaged in the PSD estimate, which causes less smoothing of the PSD estimate. This problem can be overcome by measuring longer data series in experimental system identification.

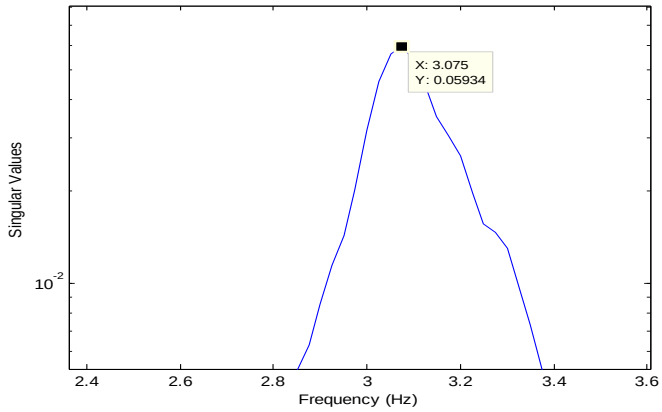

Figure 3.5 First mode frequency

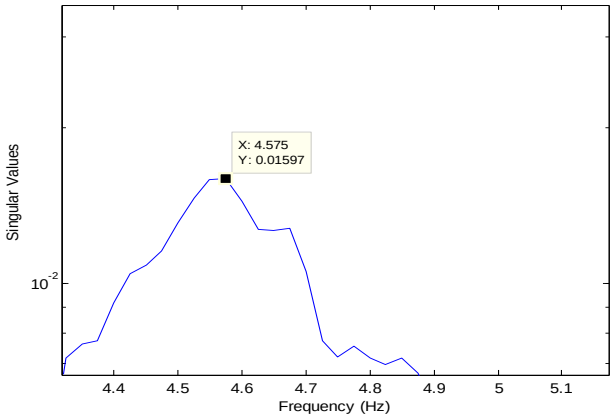

Figure 3.6 Second mode frequency

Table 3.2 indicates that the three system identification methods presented here yields good results for the 2-DOF spring-dashpot model simulation. Although the average error in

Monte Carlo simulations for damping ratios is low both for ERA and COV-SSI, in Figure 3.2 and Figure 3.3 it can be seen that damping estimation of COV-SSI might be erroneous, but ERA results are more consistent in both damping and frequency estimation.

Table 3.2. Modal Parameter estimation results for the three system identification methods

	MAC	Freq(Hz)	Error (%)	Damp (%)	Error (%)
PSD	0.95	4.58	0.44	-	-
	0.9	3.08	-0.52	-	-
ERA	0.97	4.55	0	0.0538	0.37
	0.99	3.09	0.09	0.0254	0.4
COV-SSI	0.99	4.55	-0.04	0.0532	-0.75
	0.98	3.09	0.06	0.0262	3.56
Actual	-	4.56	-	0.0536	-
	-	3.09	-	0.0253	-

The identification simulations in this part show that ERA, FDD and COV-SSI are robust identification schemes when white-noise input is applied to the model. In the following sections, the identification methods will be used with the forced vibration test simulation data.

3.2. Finite Element Building Model and Identificaiton with Eccentric Mass Shakers

To simulate forced vibration tests, a finite element building model is created in the finite element structural analysis program SAP. The building model is a 3-storey, 3-by-5 bay reinforced concrete building. A three dimensional model of the building is shown in Figure 3.7. The building model is set up with the diaphragm storey level assumption, in which all the mass of a storey is concentrated at the mass center of the storey and the floor is rigid with only the in-plane DOFs (two translations and one rotation) active. The concrete type used in the finite element model is C30 and the steel type is S420.

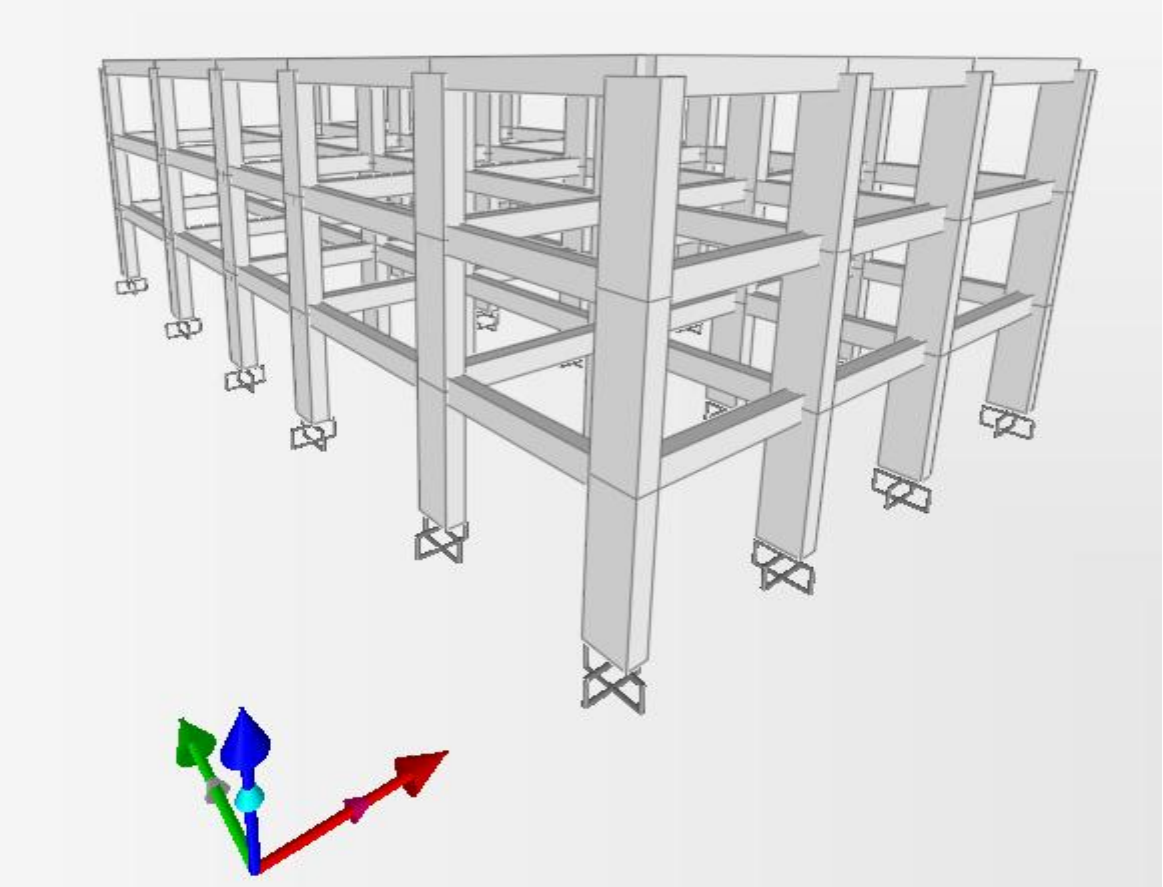

Figure 3.7 Three dimensional view of the finite element building model

In Figure 3.9, the plan view of storey levels is illustrated. In this figure, point S is the point where the force is applied at the third storey level of the finite element model. This is the point where in actual experiments a shaker can be placed. The force is applied at a 45° direction as if the shaker is located in this direction to excite the building both in N-S and E-W directions. Since the point where the force is applied is not at the center of the storey, the torsional modes of the model are excited as well.

In Figure 3.9, A, B, C and D are the points where the output time history functions are taken from the finite element analysis. Since in real life experiments it is not possible to measure the rotation directly from the center, to be able to find the rotational acceleration of the center, the accelerations in N-S direction are taken from the points A and B, and accelerations in E-W directions are taken from the points C and D. The accelerations in N-S and E-W directions and rotation in vertical direction are calculated as

$$\begin{aligned} y_{N-S} &= (y_A + y_B)/2 \\ y_{E-W} &= (y_C + y_D)/2 \\ y_Z &= (y_A - y_B)/2l \end{aligned} \tag{3.2}$$

where l is the distance from the measurement point to the center of the building, y_A, y_B, y_C and y_D are the measured accelerations. The time history data taken from the finite element analysis are first contaminated with 5% noise content and, then the data are used to calculate the accelerations of the center.

Like the other identification methods in the literature, the ERA/ARX requires the input data be a white-noise series. By imposing this property to the input applied to the structure, it is guaranteed to have significant contribution of all modes of the structure to the output, which is equivalent to imposing observability condition to the output. When an ARX model is being derived from an input-output set, the aim is to have a mathematical model that has same input-output mapping with the actual system and to produce pulse response sequence from the estimated ARX model. So the output data used in derivation of the ARX model must include response of all modes of the structures. Theoretically, every type of input to a linear dynamic structure excites all modes of the structure. This property is illustrated with Figure 3.10. The response of one DOF of a 2-DOF spring dashpot system to a sinusoidal input with 1 second period and PSD of the output is given in the figure. As can be seen in the figure, the response function contains signals with 1 Hz frequency, which is the steady state part of the output, and signals with 3.06 and 4.56 Hz, which are the mode frequencies of the system. The real life applications contradicts with the previous clause, because the real life data contains noise, which might have higher amplitude than weakly excited modes. Another point to be mentioned is that in stepped-sine tests, a sinusoid is applied to the system and only the steady part of the data is recorded, which means that the transient part of the output data is missing. The steady-state data contains information only about the magnitude of the FRF at a frequency point and this kind of input-output data is not adequate to derive an ARX model of a linear dynamic structure. To illustrate this clause, a sine wave is applied as an input to a 2-DOF spring-dashpot system and an ARX model is set up with the steady-state response of the spring-dashpot system to the sine wave. Recall from Equation (2.46) that to find the coefficients of an ARX model, inverse of $\Xi\Xi^T$ is to be calculated. However in Figure 3.8, it can be

seen that this inverse cannot be calculated because the singular values of the $\Xi\Xi^T$ are very small, and thus computing the coefficients of an ARX model with a single sine wave becomes a numerically unstable problem.

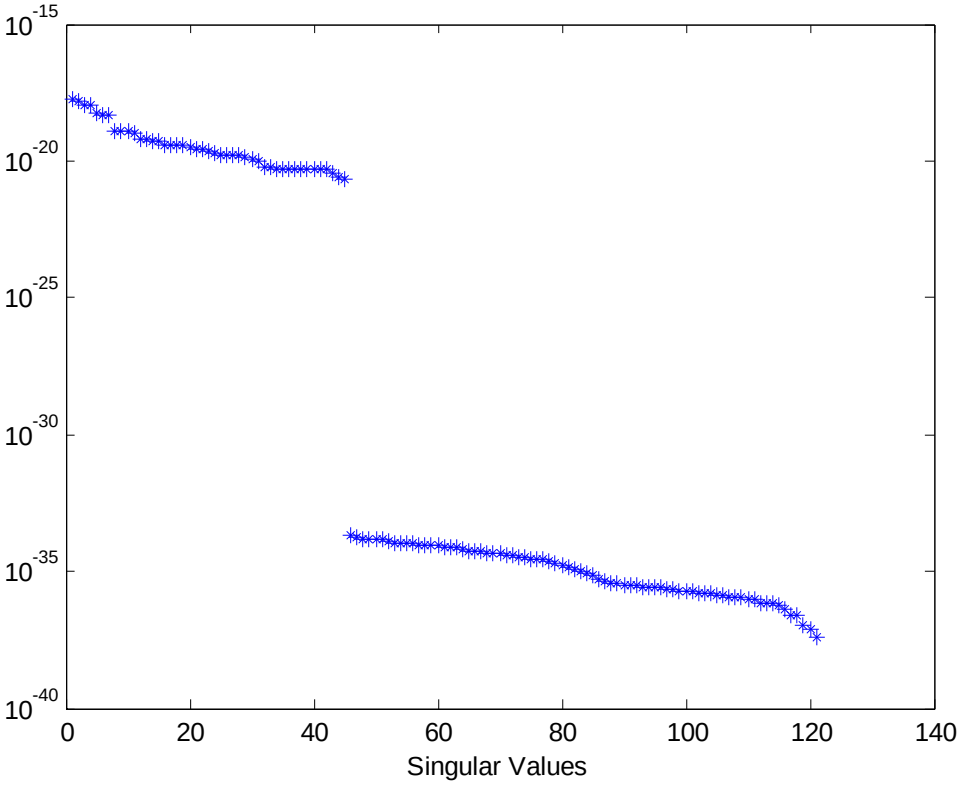

Figure 3.8 Singular Values of $\Xi\Xi^T$

Since sinusoidal inputs are not suitable to use in ERA, in order to use ERA with FVT data for identification, a simple modification of data is needed. As mentioned before, the forced vibration data generated with eccentric mass shaker provides sinusoidal inputs applied to the system at frequency steps and the responses measured at this frequency steps. The steady-state response of the system and the corresponding input is recorded in forced vibration tests. In Figure 3.11, a sample data recorded in FVT is shown. The part before first dashed line contains transient response which means the system is not at steady state. In forced vibration tests, the part between the dashed lines, the steady-state response is recorded to be used in system identification. A sinusoidal input and corresponding steady-state output is recorded at each frequency step in FVT. The idea that is going to be

used in this study to use FVT data in ERA is to sum up sinusoidal input data and corresponding output data to obtain a single data series for input and each output channel.

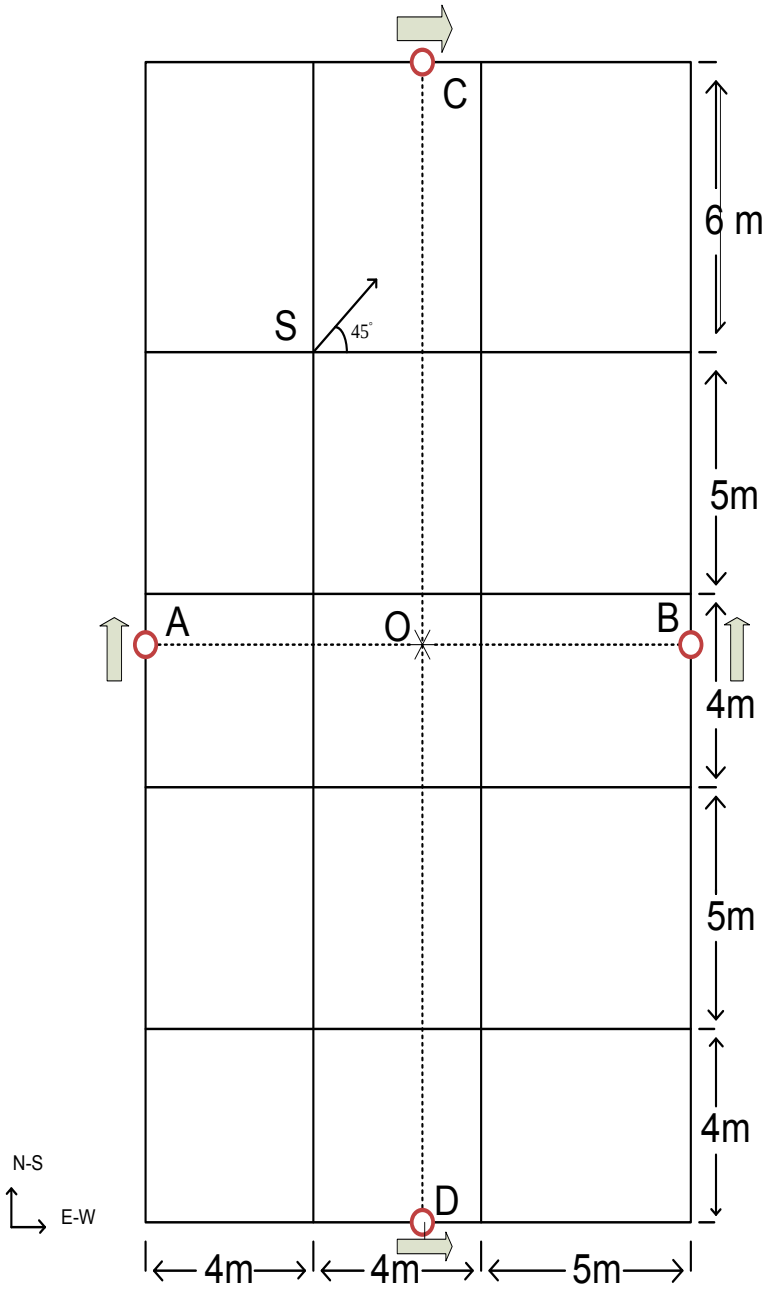

Figure 3.9. Plan view of the building model

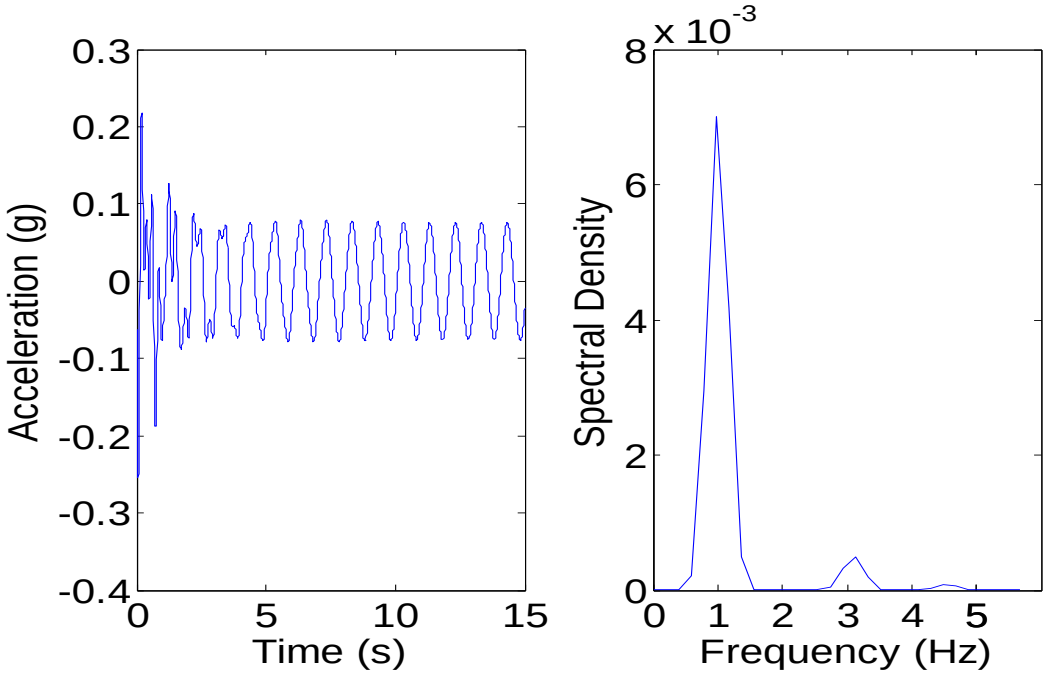

Figure 3.10. Response of one DOF of a spring dashpot system to a sinusoid

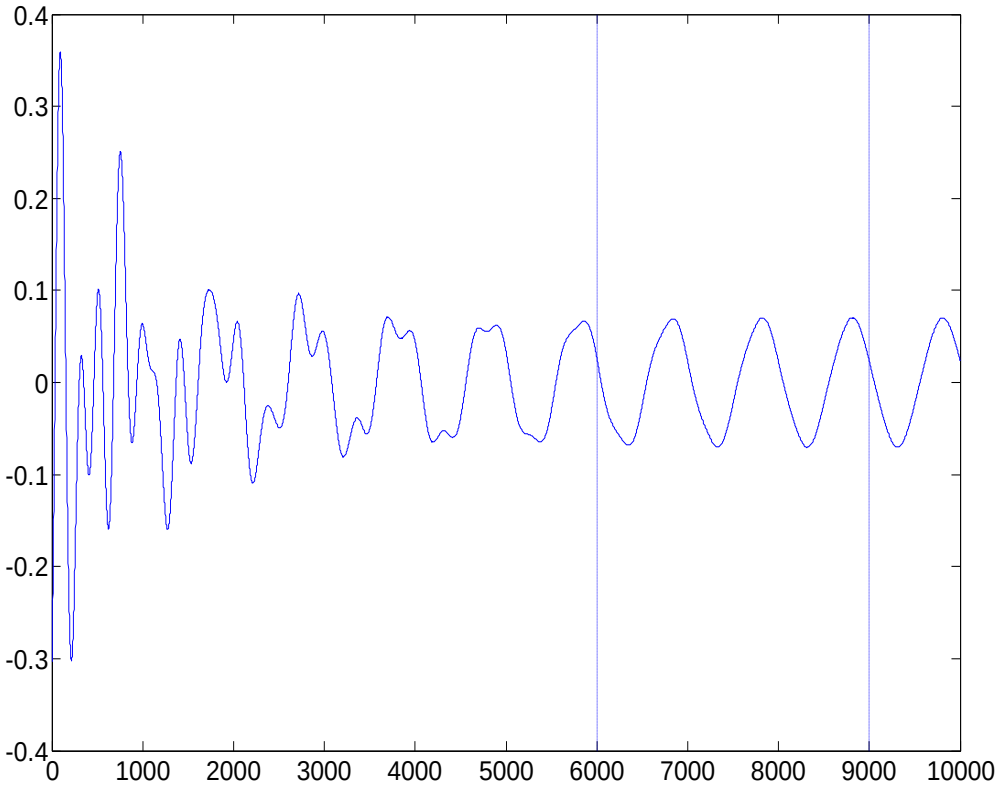

Figure 3.11 Forced Vibration Test Data

To illustrate the aforementioned idea, three sinusoidal inputs are applied to a linear dynamic system and the steady-state responses and corresponding parts of the input data are plotted in Figure 3.12. The inputs and outputs are typical forced vibration test outputs. Since a white-noise is a signal having equal contribution of all frequencies in frequency spectra, it can be said that if a stepped sine test can be conducted through zero and plus infinity, then, when the input sinusoids are summed, a white-noise like data will be obtained. Practically in a FVT, it is impossible to scan frequencies from minus infinity to plus infinity but still if all the input and output data are added separately, the resulting data sequence will be similar to white-noise, and will contain responses of all modes in and around the scanned frequency interval. This idea will be used in this section to use FVT data in system identification with ERA, as in Figure 3.12.

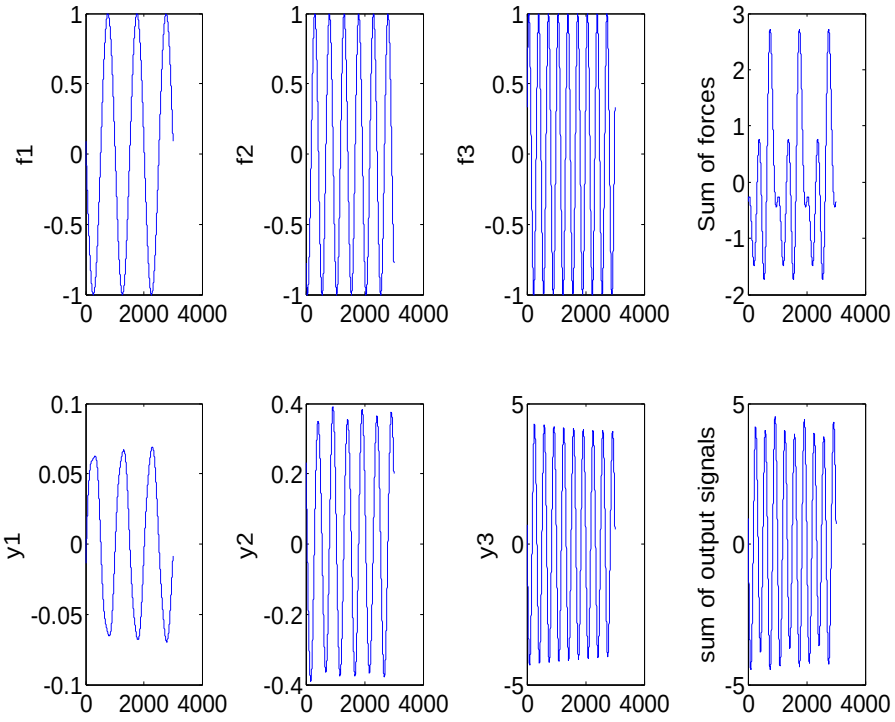

Figure 3.12 Input forces and corresponding output signals

To show the effect of adding steady-state responses of a system to individual sine waves, sine waves with different frequencies are applied as an input to a 2-DOF spring dashpot system, then ARX models are set up with the steady-state response and input. At

each step a new sine wave is applied and steady-state response to this sine wave is added to response data and corresponding input is added to input data. 40'th order ARX models are created with one sine wave data to two hundred sine wave data. As can be seen in Figure 3.13, prediction error norms of ARX models are extreme until the number of different sine waves present in the data set reaches 20. After this point, prediction error norms decrease with number of sine waves present in the data. It is obvious that until the sharp decrease, because of the numerical instability, the estimated ARX models does not represent the properties of the system. The point where the prediction error norm drops depends on the frequencies of the sine waves present in the data. Scanning the mode frequencies and having scattered frequencies decreases the number of sine waves necessary for obtaining satisfactory output prediction. This shows that system identification with a single sine wave is impossible both because the numerical instability and violation of the observability condition.

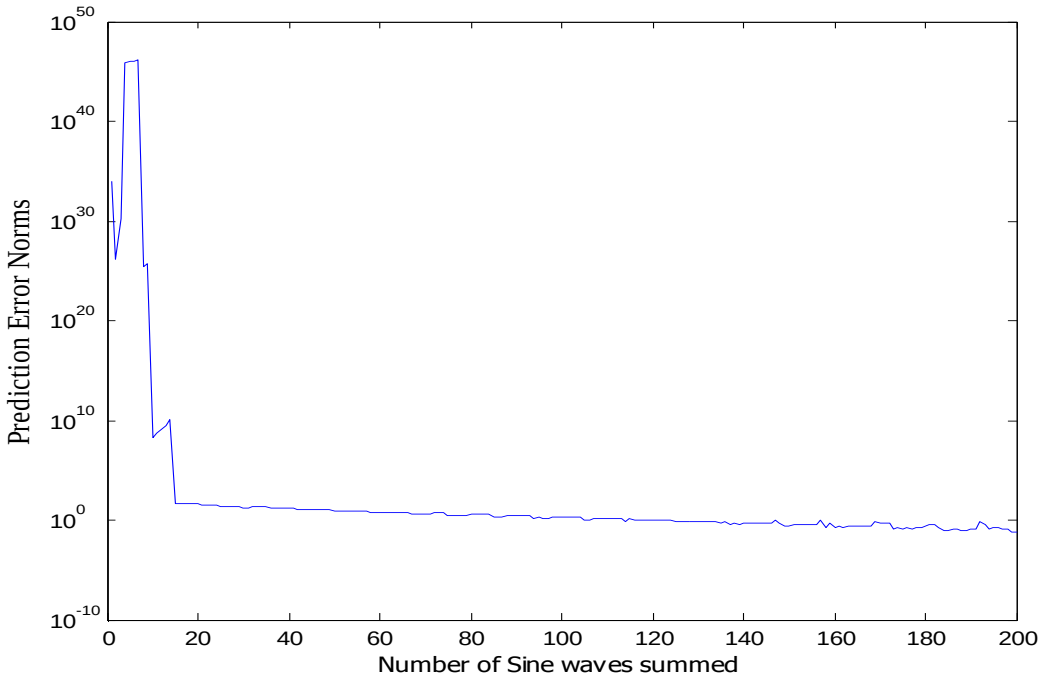

Figure 3.13. Prediction Error Norms of 40'th order ARX models set up by adding up individual sine waves

While applying the idea in Figure 3.12, amplitudes of the input forces should be normalized to 1 in real life experiments to have equal contribution of all frequency steps.

The amplitude of the input force in a FVT conducted with eccentric mass shakers is given by the formula,

$$F = m \times e \times \omega^2 \tag{3.3}$$

where m is the mass, e is the eccentricity of the masses and ω is the frequency of the input. Since the structural system is assumed to be linear, the input force can be normalized by dividing both the input and the output with the amplitude of the force F, at each frequency step.

3.3. Using FVT data with ERA

In simulation of forced vibration tests applied to the 3 storey building model, sinusoidal time history functions from 1 Hz to 21 Hz is generated with 0.1 frequency step. Each input sinusoid has 100,000 data points with 0.001 sampling time. Then, these sinusoids are fed to the finite element model as time history functions and time history responses from linear analysis are recorded. 210 input sinusoids are added up and response functions are added up after being contaminated with 5% noise. After doing this, a data set is obtained to be used in deterministic ERA. Since only steady state parts of the data can be measured, first 20,000 data points are cut off and remaining the 80,000 data points are used in ERA.

Data is resampled with 0.01 sampling time, an ARX model of 100'th order is obtained, and then with the impulse response functions generated by the ARX model, a 400-by-200 Hankel matrix is created, and state-space models from 200 to 50 order are identified. The stabilization diagram illustrated in the Figure 3.14 belongs to identification with ERA.

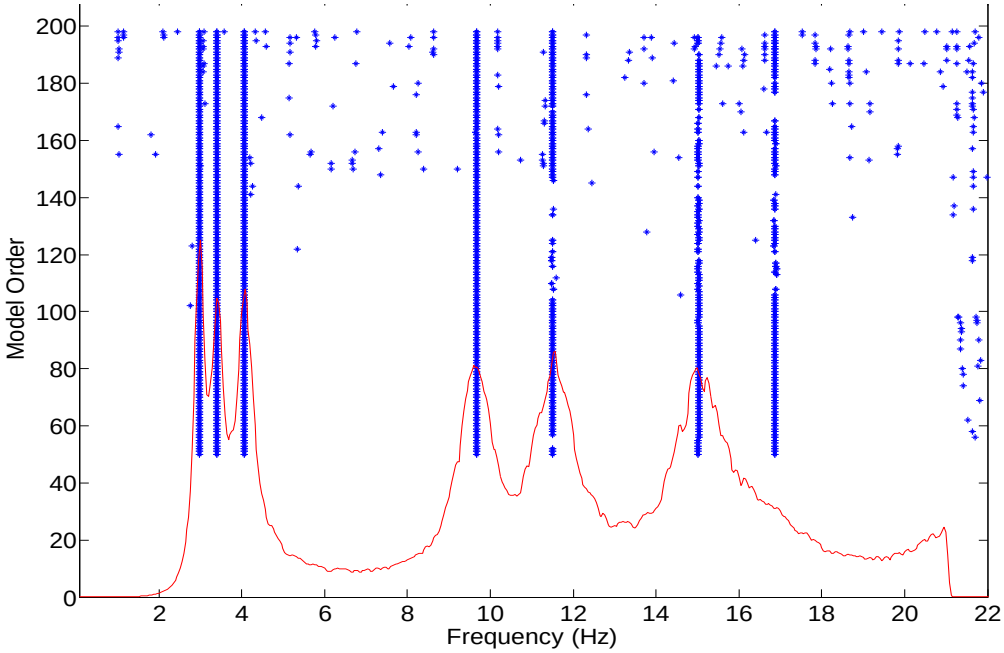

Figure 3.14 Stabilization Diagram obtained with ERA for 3 storey building model simulation

The continuous line in the Figure 3.14 is the averaged normalized power spectral density functions of output channels. By visual inspection of Figure 3.14, 7 of the 9 modes of the 3 storey building model can be identified. Since two of the modes are weak modes that have low signal amplitude in the output data, as also observed by inspection of the averaged normalized spectrum, they cannot be distinguished from noise modes.

In Table 3.3 the estimated modal parameters of the 3-storey building estimated with ERA are given. The identification error for natural frequencies are lower than 0.2 % for the first seven modes of the building, the errors are lower than 0.1 % for damping ratios , and MAC numbers are almost 1 for the 7 identified modes. The modes at 21.35 and 30.32 Hz are contained in the identified state-space models but in real test applications it will be impossible to choose such weak modes among the noise modes. It is worth noting that, since the stepped frequency interval is 1-21 Hz in the test simulations, the stabilization diagram in this interval is given. However, the rest of the stabilization diagram contains correct values of other 2 modes, but since the signal amplitude from these modes are weak, stabilization diagram is not clear in the higher frequency range. The stabilization diagram and the results show that the proposed methodology can be easily used for system identification of buildings with ERA after obtaining FVT data.

Table 3.3. Modal Parameters estimates for 3 storey building model with ERA

		Mode 1	Mode 2	Mode 3	Mode 4	Mode 5	Mode 6	Mode 7	Mode 8	Mode 9
Actual	Freq	2.98	3.40	4.07	9.67	11.51	15.04	16.89	21.35	30.32
	Damp	0.05	0.05	0.05	0.05	0.05	0.05	0.05	0.05	0.05
ERA	Freq	2.98	3.40	4.07	9.66	11.50	15.02	16.86	-	-
	Damp	0.05	0.05	0.05	0.05	0.05	0.05	0.05	-	-
Error (%)	Freq	-0.08	-0.14	-0.07	-0.07	-0.05	-0.08	-0.15	-	-
	Damp	0.20	0.80	0.20	0.20	0.80	0.00	0.80	-	-
	MAC	1.00	1.00	1.00	1.00	1.00	1.00	1.00	-	-

In Figure 3.15, actual mode shapes of the 3 storey building model are illustrated. The solid lines are displaced shapes of the each storey level. The modes at the first column in the figure are the first three bending modes of the building in E-W direction, the second columns is the first three torsion modes of the building and the last column is the N-S bending modes of the structure. To compare visually, in Figure 3.16, the modal displacements are given for the 7 modes that are identified with ERA. Both in Table 3.3 and in Figure 3.16 it can be seen that the identified frequencies and mode shapes are very accurate.

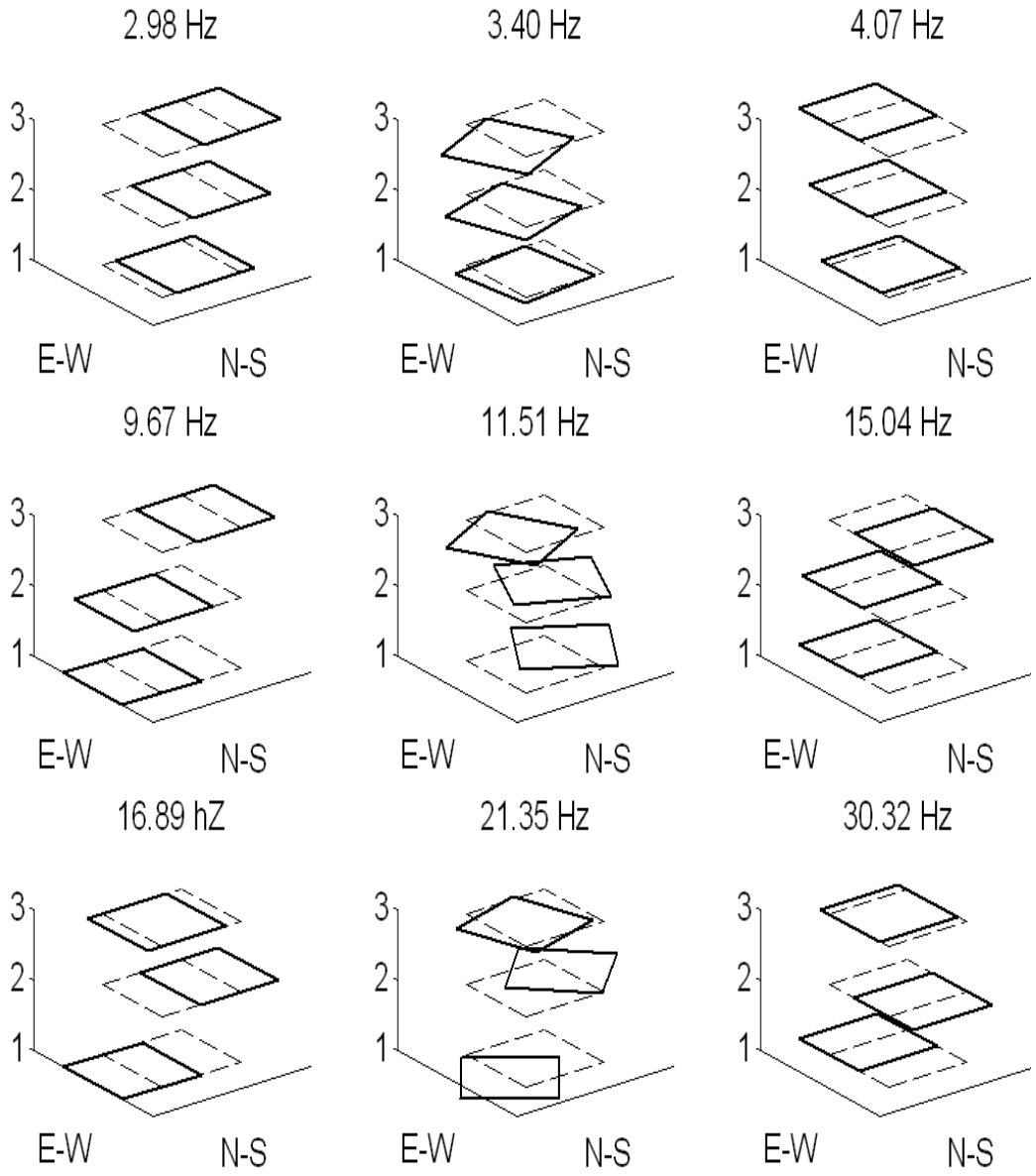

Figure 3.15 Actual mode shapes of the 3 storey building model

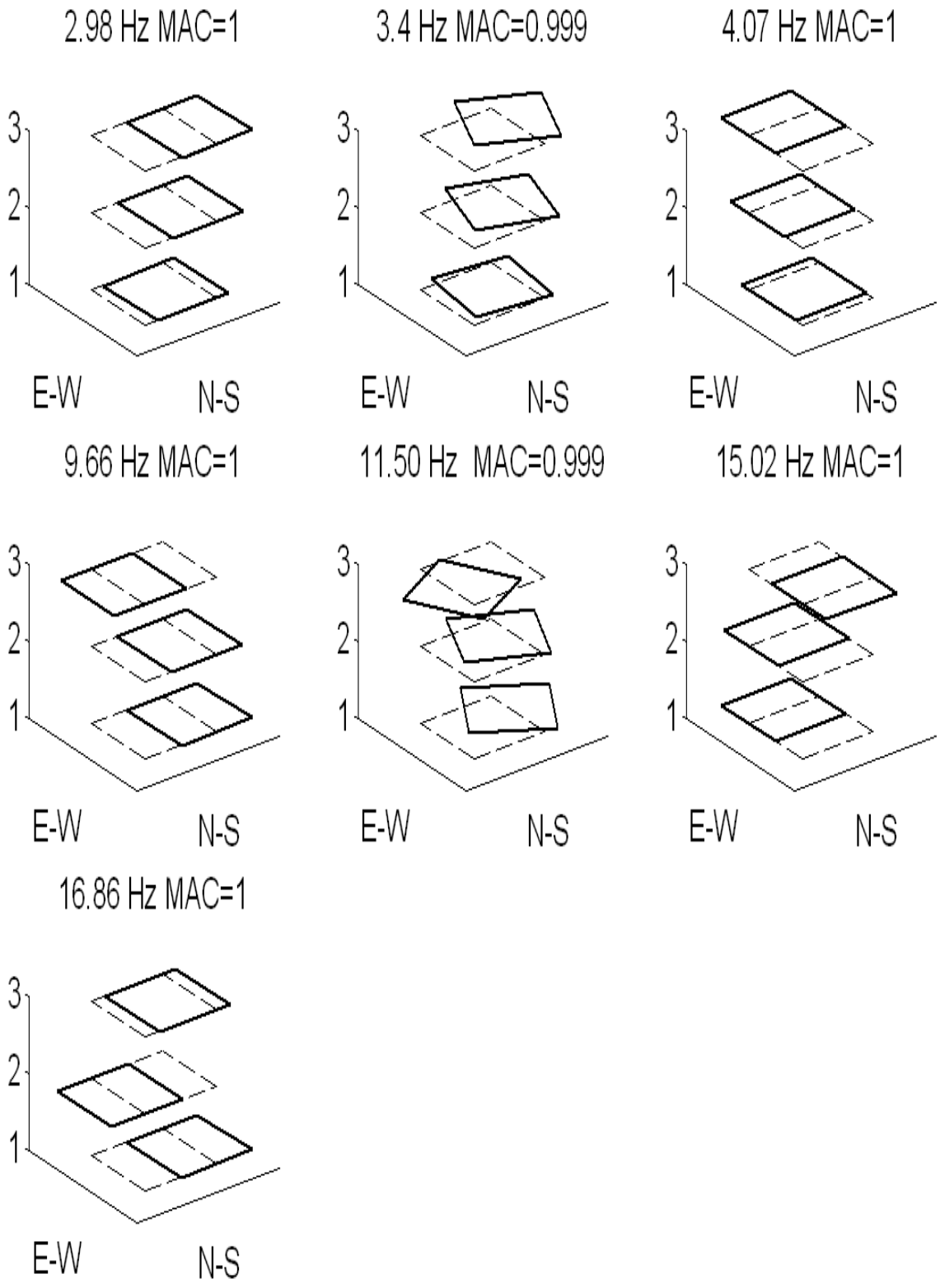

Figure 3.16. Identified mode shapes of 3 storey building with ERA

Another check for mode vector estimates in system identification is made by checking the phase angle of the estimated complex mode vector. Each mode of a classically damped system reaches its maximum at each spatial sampling point at the same time. Having phase differences far from 0 or $\pm\pi$ means that each spatial point reaches its maximum at different times, this is an indicator of mistake in identified mode shape and/or damping ratio (Luş et al, 2002). In Figure 3.17, the phase angles of the identified mode shape components of the first three modes are plotted onto the unit circle. All of the phase angles are close to 0, thus the estimated mode shapes components reach their maximums at the same time, and the system can be considered as classically damped.

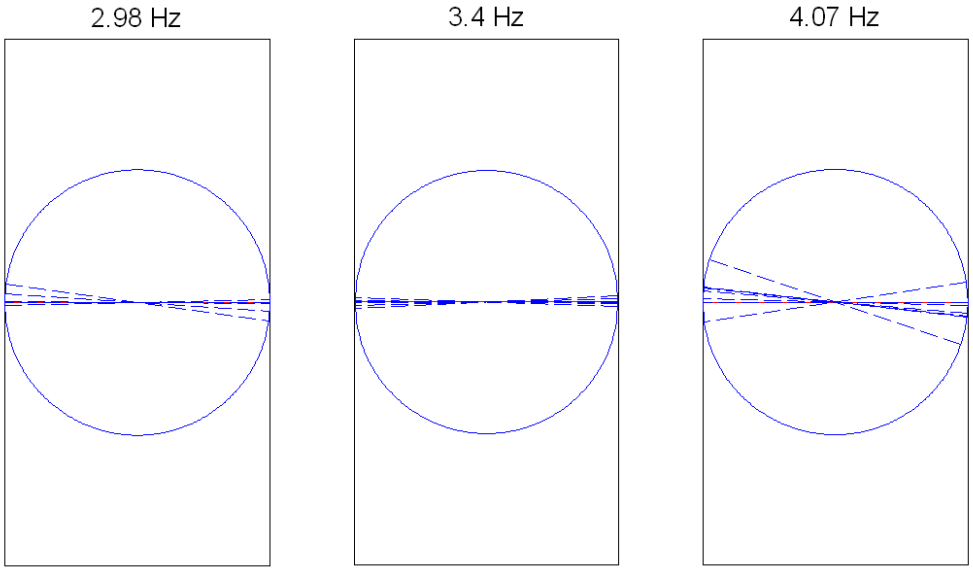

Figure 3.17. Phase angle of the identified mode shape components

3.4. Using FVT data with FDD

The finite element building model described in the previous section is used to simulate FVT for FDD. The response data simulated and previously used with ERA is used with FDD in this section. It is worth noting that in FDD case, although the amplitude of the force can be calculated with Equation (1.1), the phase difference between input and output is not known. Phase difference is the delay between input and the response when a periodical input is applied to the system. This delay of response is related with the damping

ratio at each mode. To illustrate this, consider equation of motion for free vibration of a SDOF system:

$$m\ddot{q} + l\dot{q} + kq = 0 \tag{3.4}$$

The solution of Equation (3.4) is as follows:

$$\begin{aligned} q(t) &= qe^{st} \\ s_{1,2} &= -\frac{l}{2m} \mp \frac{\sqrt{l^2 - 4km}}{2m} \\ &= -\bar{\omega}_0\zeta \mp i\bar{\omega}_0\sqrt{1-\zeta^2} \end{aligned} \tag{3.5}$$

where s is a complex number. The phase angle between input and output is the angle of the complex number s. As can be seen in Equation (3.5), this angle is related with the damping ratio of the system.

The 80,000 point output data is fed to FDD, data is windowed with 10000 point Hanning window, and 50% overlap is used in the PSD estimation. The resulting singular value spectrums are given in Figure 3.18. Four peaks in the first singular values and one peak of second singular values at the dip of first singular values are chosen as mode frequencies and corresponding left singular vectors are mode vectors of the system. Thus 5 modes of the system could be identified with the FDD method. To improve results and identify the mode vectors of the system, step size of data should be decreased; however in real life applications the step size of eccentric mass shakers can be decreased up to 0.1 Hz. Thus, the step size was chosen as 0.1 Hz, because smaller step might be inapplicable with eccentric mass shakers.

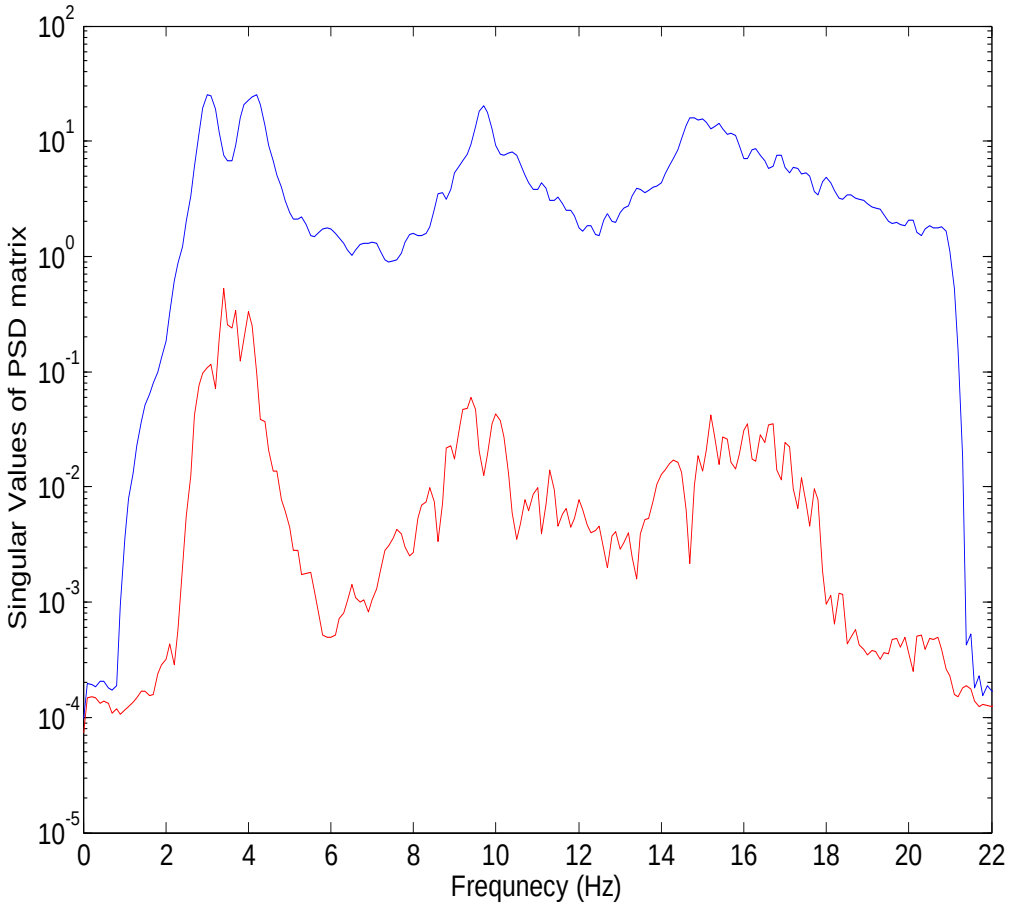

Figure 3.18. First and second singular values of output PSD matrix (Upper line is the first singular values)

Table 3.4. Modal Parameters estimates for 3 storey building model with FDD

		Mode 1	Mode 2	Mode 3	Mode 4	Mode 5	Mode 6	Mode 7	Mode 8	Mode 9
Actual	Freq	2.982	3.404	4.070	9.671	11.509	15.036	16.886	21.351	30.324
	Damp	0.050	0.050	0.050	0.050	0.050	0.050	0.050	0.050	0.050
FDD	Freq	3	3.4	4.2	9.7	-	14.8	-	-	-
	Damp	-	-	-	-	-	-	-	-	-
Error (%)	Freq	0.610	-0.129	3.192	0.297	-	-1.570	-	-	-
	Damp	-	-	-	-	-	-	-	-	-
	MAC	0.9999	0.7109	0.9946	0.9998		0.9911			

In Table 3.4, it can be seen that five natural frequencies are identified and the highest per cent error for an identified frequency is 3.5 %. Since the error in damping estimation is very high, identified damping ratios are not interpreted in the table. The MAC coefficients are almost one except the first rotation mode. As can be seen in Figure 3.19 and Figure 3.20, 4 peak points of highest singular values and one peak point of second singular values is chosen. All of the peak points in highest singular values denote a mode in the singular values plot, and while the peaks that coincide with the dip of first singular values are indicators of a mode, the other peak points in second highest singular values plot are not indicators of modes (Michel et al., 2008). When there are more than one structural mode in a small frequency range, and when these modes are orthogonal, meaning zero or very small mode coupling, the first highest mode vector shows the contribution of one of the orthogonal vectors to the FRF and the second highest mode vectors show the contribution of the other orthogonal vector. However, when there is high mode coupling and close modes, the identified mode vectors are a linear combination of two mode vectors and a peak in second highest singular values plot does not exist. In the 3 storey building model case, there are three close modes, but because there is low mode coupling, the modes at 2.98, 3.4 and 4.07 Hz are identified. The MAC values of identified mode shapes are close to 1 except the torsion mode at 3.4 Hz.

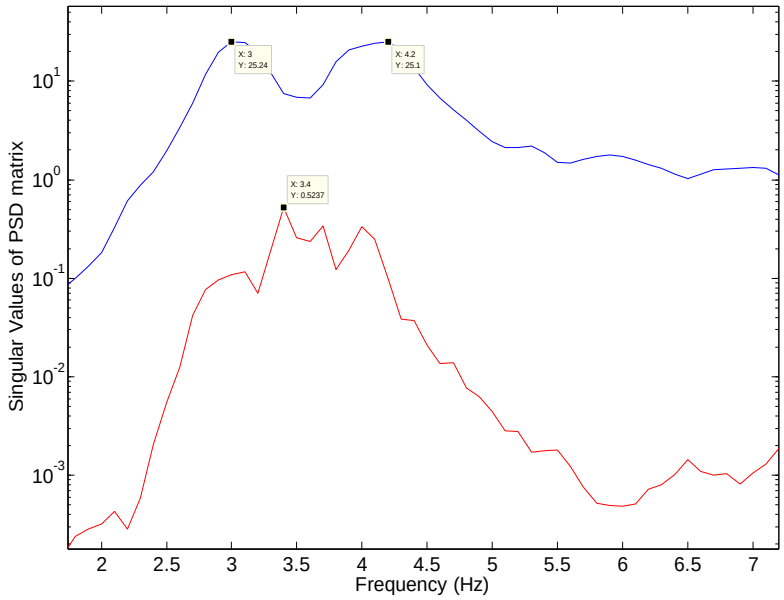

Figure 3.19. First three peaks chosen as mode frequencies of 3 storey building

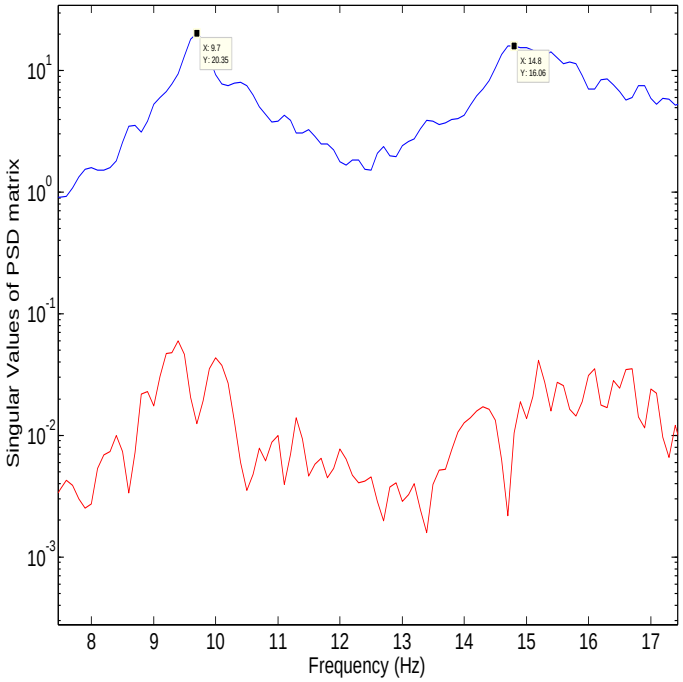

Figure 3.20. Fourth and fifth peaks chosen as mode frequencies of the 3-storey building

When the estimated mode shapes in Figure 3.21 are compared with the actual mode shapes in Figure 3.15, it is seen that the first two bending modes in N-S and E-W direction are estimated correctly. The first torsion mode which has 0.7 MAC value the corresponding actual mode seems like a bending-torsion mode, although the actual mode shapes are orthogonal. Thus, it can be concluded that closely spaced modes and mode coupling decreases identification accuracy in the FDD method.

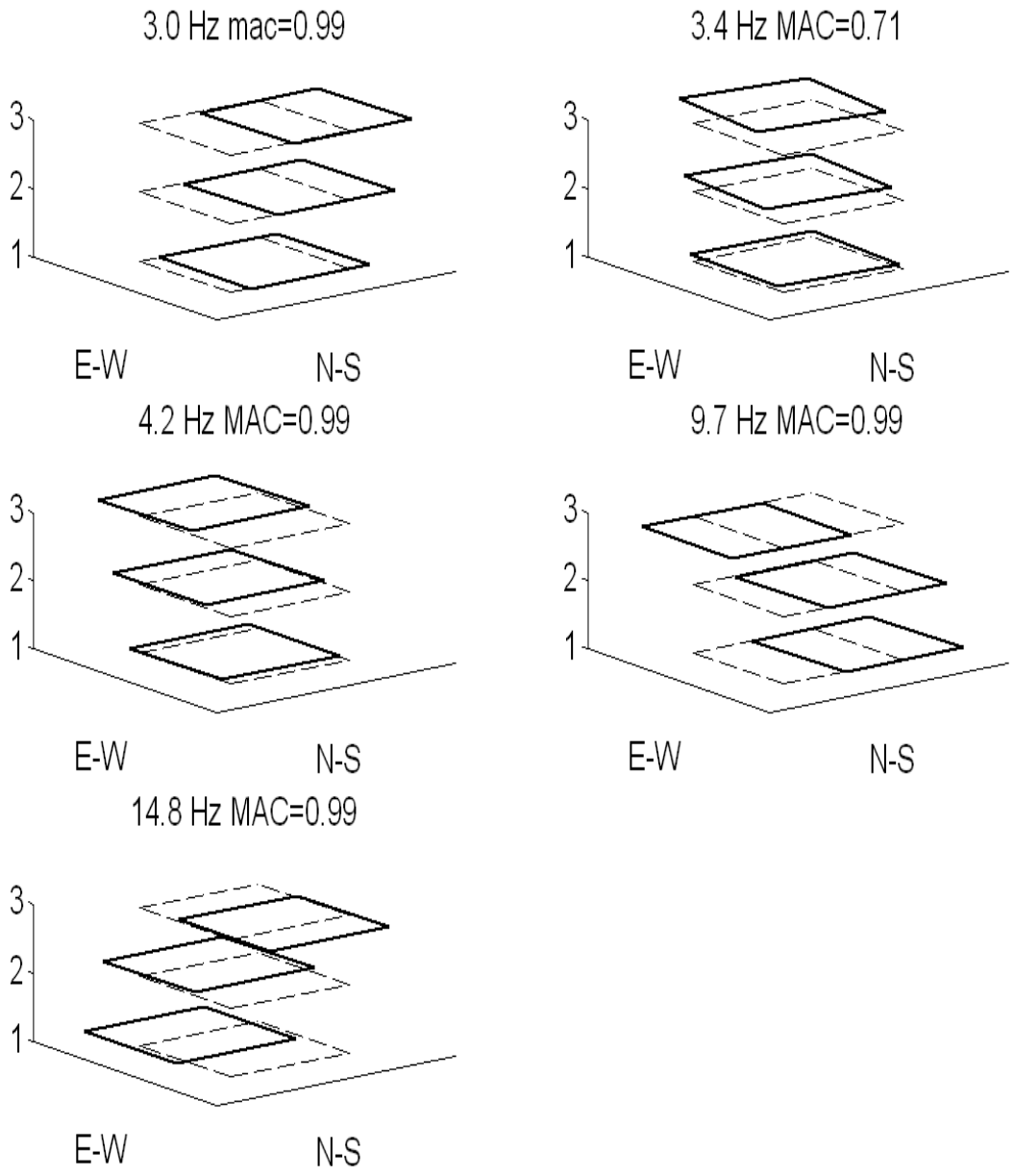

Figure 3.21. Identified mode shapes of 3 Storey building with FDD

In Figure 3.22 the phase angles between the identified mode shape components are plotted for the first three modes. There are more than phase differences exceeding $\pi/4$ between the components for the first and the third modes, which are the first bending modes along N-S and E-W directions respectively. The plots show that the damping estimation is highly erroneous with the FDD method.

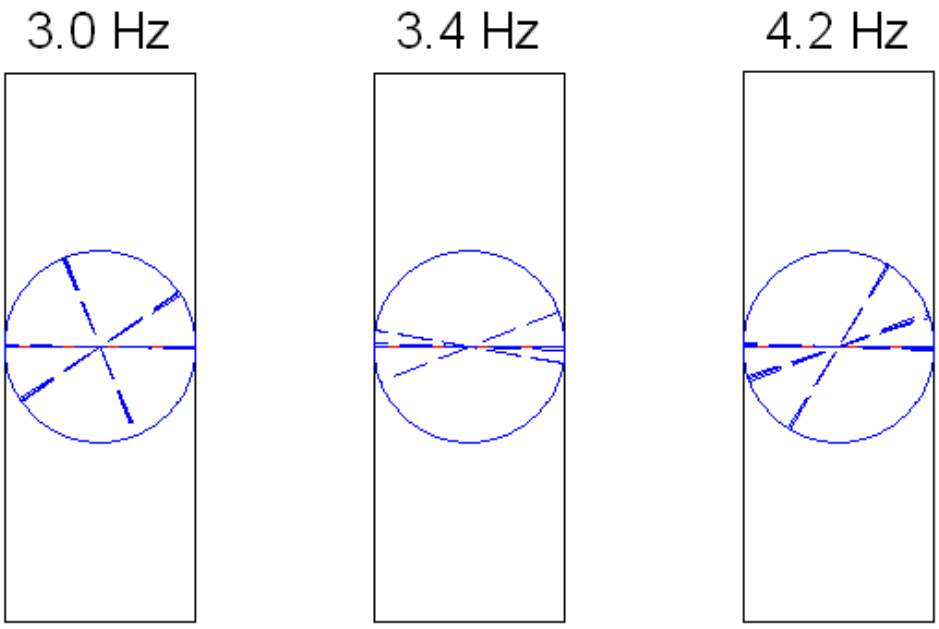

Figure 3.22 Phase angles of the identified first three mode shape components

3.5. Using FVT data with COV-SSI

In this section, forced vibration data is modified to use with the COV-SSI method for system identification. For the COV-SSI method, in place of making a stepped sine test, the eccentric mass shaker can be used as a sine-sweep machine. To simulate this condition, a sinusoidal chirp is simulated as input. In Figure 3.23, an example of sine chirp is plotted. A sine sweep test, conducted by using eccentric mass shaker manually and changing the frequency randomly, is simulated in this chapter. An input force changing the frequency four times is applied to the finite element building model used for other identification methods; input time history functions are recorded as input measurements, and response of the building to this sine chirp force is recorded as output data. While applying this methodology for system identification with COV-SSI, the system identification accuracy decreases if the number of target frequencies increase enormously. In this case, the mathematical modes start to be stable as if they are system modes. Thus the physical modes cannot be distinguished from mathematical modes. So in the simulations, target frequency is changed 4 times.

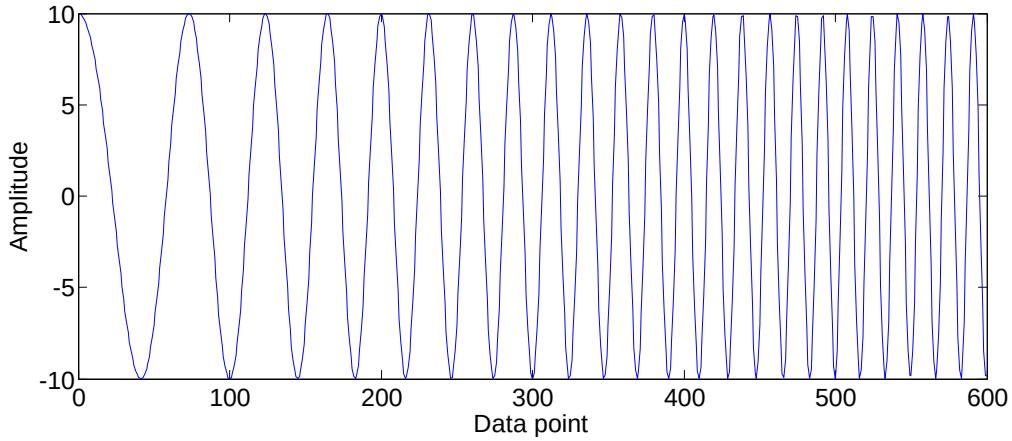

Figure 3.23. Sine chirp time history

In simulations, 40000 data points are created with 0.001 sampling time. First 10000 of the data points are not used in system identification because in simulation the building starts from zero initial conditions; however, this is not the case in real life conditions. The time history functions are resampled with 0.01 sampling time and filtered with Chebishev filter. 50-by-9 lag covariance functions are calculated, and a 450-by-450 Toeplitz matrix is created. It is worth noting that, until some point, increasing covariance lag increases the accuracy of the COV-SSI method but when the lag is increased too much, noise modes become stable and distinguishing noise modes and physical modes gets hard. To find the best stabilization diagram, covariance lag should be changed while keeping other parameters constant. The state-space models from 200 to 50 order are identified with the COV-SSI. In Figure 3.24, the stabilization diagram obtained with COV-SSI method is plotted. The averaged normalized spectrum is not plotted on to the stabilization diagram, because the input signal is neither white-noise nor white-noise-like data, such that the spectrum does not have to have peaks at the natural frequencies of the system.

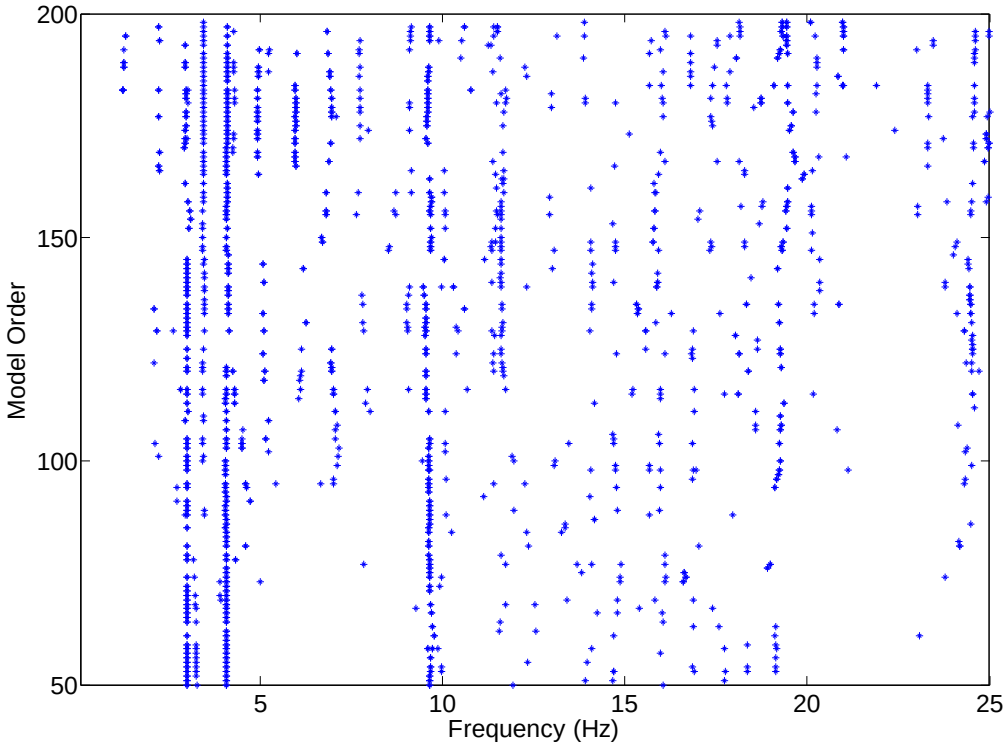

Figure 3.24 Stabilization diagram for the 3-storey building model identified with COV-SSI

Table 3.5 Parameter estimates for the 3 storey building model with COV-SSI

		Mode 1	Mode 2	Mode 3	Mode 4	Mode 5	Mode 6	Mode 7	Mode 8	Mode 9
Actual	Freq	2.982	3.404	4.070	9.671	11.509	15.036	16.886	21.351	30.324
	Damp	0.050	0.050	0.050	0.050	0.050	0.050	0.050	0.050	0.050
COV-SSI	Freq	3.00	3.25	4.07	9.66	-	-	-	-	-
	Damp	0.03	0.05	0.05	0.05	-	-	-	-	-
Error (%)	Freq	0.741	-4.503	-0.042	-0.125	-	-	-	-	-
	Damp	-44.600	-2.200	-1.200	2.400	-	-	-	-	-
	MAC	0.9996	0.2116	0.9994	0.9996					

Table 3.5 shows the estimated modal parameters with the COV-SSI method using outputs of the sine sweep simulation. Four of the nine modes are identified with COV-SSI.

Percent error is lower than 1% for frequency estimates of three modes, but for the mode at 3.4 Hz the error is 4.5% and the error in the damping ratio estimate is 44.6%. The MACs of the estimated mode vectors are close to 1 except the mode at 3.4 Hz. Thus, modal parameters of 3 modes are estimated well, but still some improvement is needed for the COV-SSI method to be applied to FVT data.

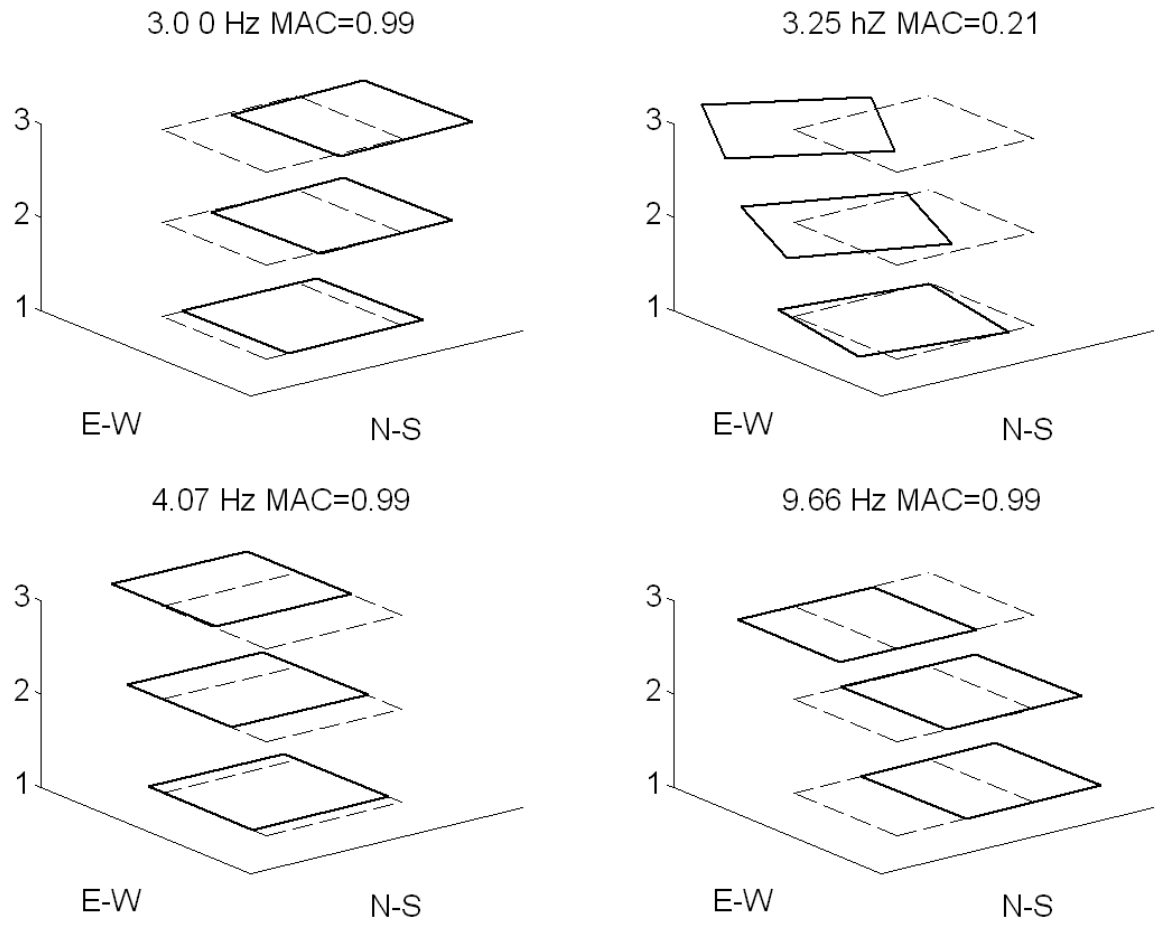

Figure 3.25. Estimated mode shapes of 3 Storey building with COV-SSI

In Figure 3.26, phase angle differences for the estimated mode shape components for the first three modes are plotted onto unit circles. From the figure, it can be concluded that the estimated complex mode vectors do not have correct phase angles because the phase angles are far from 0 or $\pm\pi$.

The estimated mode shapes in Figure 3.25 fits quite well with the actual mode shapes except for the mode at 3.25 Hz. Apparently this is the first torsion mode at 3.4 Hz, however the deflection pattern is not similar with the actual mode shape.

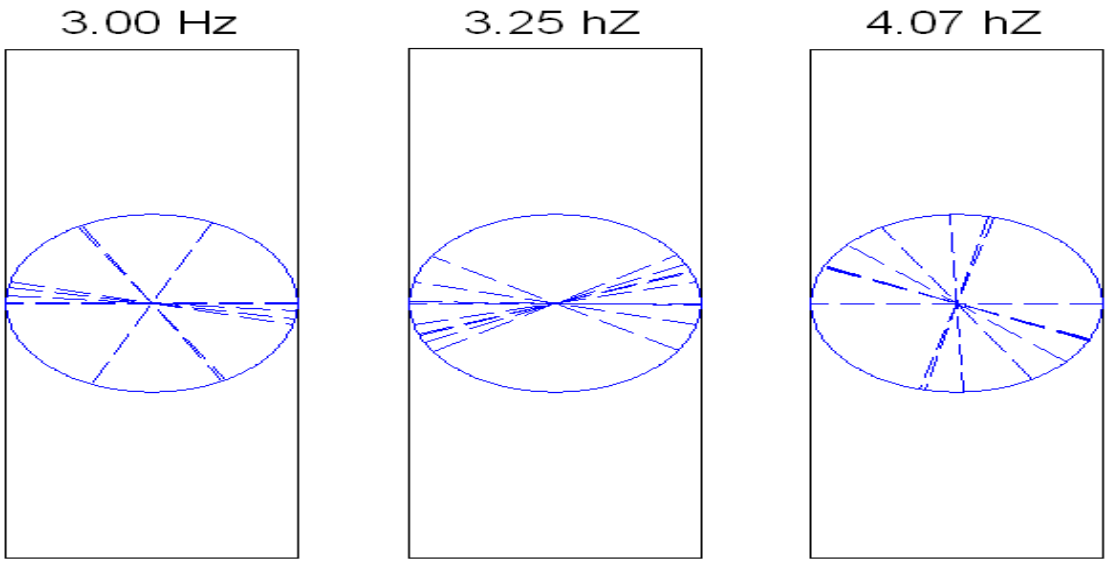

Figure 3.26. Phase angle of the identified first three mode shape components

When modal parameter estimates of the three algorithms with proposed methods are taken into account, it is obvious that ERA method is superior than the FDD method and the COV-SSI. The damping estimate with FDD is introduced in Chapter 2; however, in the analysis it has been seen that damping estimates of FDD are highly mistaken. On the other hand damping estimates of ERA and COV-SSI are quite accurate for the modes identified. It should be noted that, in the finite element model analysis, the assumptions of linearity and classical damping are not violated. However in real life applications of the proposed methodologies with eccentric mass shakers, there will be nonlinearities in the observed data, the noise content in the data will not be perfectly uncorrelated white-noise and in sine sweep, the change of the speed in the shaker motor will not be linear as well; therefore the assumptions will be violated to some extent. This contradiction in real life applications with simulation will certainly decrease the accuracy of the identification schemes, and especially the damping estimates may be expected to be in more error.

4. CONCLUSION AND RECOMMENDATIONS

The purpose of this study was to investigate system identification strategies for identifying modal parameters of actual buildings with forced vibration tests conducted with eccentric mass shakers.

Three system identification methods were introduced in this study to be applied with forced vibration test data. To investigate the accuracies of the identification methods, a Monte Carlo simulation is done with a 2-DOF spring-dashpot system. The results of the Monte Carlo simulation show that the performance of the ERA/ARX, the COV/SSI and the FDD is satisfactory in terms of mode frequencies and mode vectors. The ERA/ARX and the COV-SSI estimate damping ratios accurately as well. However the damping ratio estimates with FDD are highly biased.

One of the fundamental problems is the determination of the physical modes among the spurious noise modes. Two strategies were used in this study. One of them is constructing a stabilization diagram. Stabilization diagrams make use of the fact that the physical modes of the system are expected to exist more consistently in a set of different model orders extracted from a given data set, but the spurious noise modes are expected to deviate more. Using this information in model order determination is proven to be useful both in this study and in the studies reported previously. The shortcoming of the stabilization diagrams is that they require experienced user interaction in physical mode determination. Due to this shortcoming, clustering algorithms which automate the mode selection process are improved by teaching the computer how to classify a mode as physical or spurious. Both stabilization diagrams and a clustering algorithm are used in this study along with ERA/ARX and COV-SSI; however, stabilization diagrams cannot be applied with the FDD. This can be stated as a drawback of the FDD, because the mode selection is done manually by the user. This requires the user to have knowledge of the FDD and modal analysis. It is worth noting that although clustering algorithms automate the identification process, still the user checks the results, because both the stabilization diagram and the clustering approaches are criticized as being heuristic methods.

,

The idea of summing up individual sine responses obtained with a forced vibration test conducted with eccentric mass shakers was applied with the data obtained from a finite element building model. In this way, the modal parameters were estimated accurately with the ERA/ARX method. Preprocessing data with decimation and filtering improved the results. Considering the analysis done with ERA/ARX, it can be said that the idea introduced in this study to apply the ERA/ARX with forced vibration test data is useful because in the studies conducted before, system identification is done with traditional peak picking method. In application of the peak picking method, too much user interaction is required and damping ratio and mode vector estimates might be highly biased. Thus, using ERA/ARX is more advantageous when both the input and the output can be measured in eccentric mass shaker experiments.

The FDD was investigated as a method to be used if the phase angle between input and output cannot be measured. The output data set used in the ERA/ARX case was also used with the FDD. It was seen that mode frequencies and mode vectors can be identified with the FDD by the proposed methodology. However, during the preparation of this dissertation, it was observed that having closely spaced mode frequencies in the frequency spectra and having high mode coupling decrease the accuracy of the FDD.

The COV-SSI method was used with the sine-sweep data generated with eccentric mass shakers. Applying decimation and filtering improves the results in the COV-SSI case more than the ERA/ARX case. The results stated in this study show that COV-SSI can be used in identification when the transient response can be measured. Applying the Canonical Variate Analysis is crucial when the COV-SSI is used with multiple sine-chirp data, as was the case in this study.

The analysis in this study showed that the proposed methodologies are satisfactory for real life applications of forced vibration tests with eccentric mass shakers. It was obvious that when both the input and the output are measured and ERA/ARX can be applied, modal parameters can be estimated better. On the other hand, COV-SSI and FDD are superior in the sense that they make it possible to identify the modal parameters when phase difference between the input and the output cannot be measured.

Further research may focus on the improvement of estimation of damping ratios with the FDD method, and the improvement of mode vector estimation when there are close and coupled modes. Identification of the modal parameters of weakly excited modes is highly biased in the COV-SSI method with the proposed methodology. Further investigations might improve the results obtained with the COV-SSI method when some modes are weakly excited.

It should be taken into account that the analysis done in this study was done with computer simulations. In the real life applications, some of the assumptions might be violated to some extent. This might decrease the parameter estimation accuracies of the proposed methods. Conducting a forced vibration experiment on a real life structure and verifying the validity and robustness of the analysis would provide a field for future research.

REFERENCES

Akaike, H., 1974, "Stochastic Theory of Minimal Realization", *IEEE Transactions on Automatic Control*, Vol. AC-19, No. 6, pp. 667-674.

Akaike, H., 1975, "Markovian Representation of Stochastic Processes by Canonical Variables", *Siam Journal on Control and Optimization*, Vol. 13, No. 1, pp. 162-173.

Arun, K. S. and S. Y. Kung, 1990, "Balanced Approximation of Stochastic Systems" *Siam Journal on Matrix Analysis and Applications*, Vol. 11, No. 1, pp. 42-68.

Alıcıoğlu, B., 2006, *Ambient Vibration Signature Analysis With Subspace Methods: Case Studies*, M.Sc. Thesis, Boğaziçi University.

Aström, K. J. and T. Bohlin, 1965, " Numerical identification of linear dynamic systems from normal operating records", *Proceedings of the IFAC Symposium on Self-Adaptive System*, Teddington, UK.

Bekey, G. A., 1970, "System Identification – An Introduction and a Survey", *Simulation*, Vol. 15, No. 4, pp. 151-166.

Brincker, R., L. Zhang and P. Andersen, 2000a, "Output-Only Modal Analysis by Frequency Domain Decomposition", *Proceedings of the 25th International Seminar on Modal Analysis*, Vol. 2, pp. 717-723, Leuven, Belgium.

Brincker, R., L. Zhang and P. Andersen, 2000b, "Modal Identification from Ambient Responses using Frequency Domain Decomposition", *Proceedings of the 18th International Modal Analysis Conference*, pp. 625-630, San Antonio, Texas.

Brincker, R., C. E. Ventura and P. Andersen, 2001, "Damping Estimation by Frequency Domain Decomposition", *Proceedings of the 19th International Modal Analysis Conference*, Vol. 1, pp. 698-703, Florida, USA.

Cooley, J.W., P. A. Lewis and P. D. Welch, 1969, "The Finite Fourier Transform", *IEEE Transactions on Audio and Electroacoustics*, Vol. 17, No. 2, pp. 77-85.

De Roeck, G., B. Peeters and W. X. Ren, 2000, "Benchmark Study on System Identification through Ambient Vibration Measurements." *Proceedings of the 18th International Modal Analysis Conference*, pp. 1106-1112, San Antonio, Texas.

Ewins, D. J., 1984, *Modal Testing: Theory and Practice*, Research Studies Press, London.

Felber, A.J., 1993, *Development of a Hybrid Bridge Evaluation System*, Ph.D. Dissertation, University of British Columbia.

Gevers, M., 2003, "A Personal View on the Development of System Identification", *Proceedings of the 13th IFAC Symposium on System* I*dentification*, pp. 773-784, Rotterdam, Netherlands.

Guyader, A. and L. Mevel, 2003, "Covariance-Driven Subspace Methods: Input/Output vs. Output-Only", *Proceedings of the 21st International Modal Analysis Conference*, Florida, USA.

Ho, B. L. and R. E. Kalman, 1965, "Effective Construction of Linear State-Variable Models from Input/Output Data", *Proceedings of the 3rd Annual Allerton Conference on Circuit and System Theory*, pp. 449-459, Illinois, USA.

Ibrahim, S. R., 1977, "Random Decrement Technique for Modal Identification of Structures", *Journal of Spacecraft*, Vol. 14, No. 11, pp. 696-700.

James, G. H., T. G. Carne and J. P. Lauffer, 1993, *The Natural Excitation Technique for Modal Parameter Extraction from Operating Wind Turbines*, SAND92-1666, UC-261, Sandia National Laboratories.

Juang, J. N., 1994, *Applied System Identification*, Prentice Hall, New Jersey.

Juang, J. N. and R. N. Pappa, 1985, "An Eigensystem Realization Algorithm for Modal Parameter Identification and Reduction", *Journal of Guidance, Control, and Dynamics*, Vol. 8, No. 5, pp. 620-627.

Kennedy, C. C. and C. D. Pancu, 1947, "Use of Vectors in Vibration Measurement and Analysis", *Journal of the Aeronautical Sciences*, Vol. 14, No.11, pp. 603-625.

Larimore, W.E., 1990, "Canonical Variate Analysis in Identification, Filtering and Adaptive Control", *Proceedings of the 29th IEEE Conference on Decision and Control*, pp. 596-604, Honolulu, Hawaii.

Lau, J., J. Lanslots, B. Peeters and H. Van der Auweraer, 2007, "Automatic Modal Analysis: Reality or Myth?", *Proceedings of the 25th International Modal Analysis Conference*, Florida, USA.

Luş, H., R. Betti and R. W. Longman, 2002, "Obtaining Refined First-Order Predictive Models of Linear Structural Systems", *Earthquake Engineering and Structural Dynamics*, Vol. 31, No. 7, pp. 1413-1440.

Magalhaes, F., A. Cunha and E. Caetano, 2009, "Online Automatic Identification of the Modl Parameters of a Long Span Arch Bridge", *Mechanical Systems and Signal Processing*, Vol. 23, pp. 316-329.

Michel, C., P. Gueguen and P. Bard, 2008, "Dynamic Parameters of Structures Extracted from Ambient Vibration Measurements: An Aid for the Seismic Vulnerability Assessment of Existing Buildings in Moderate Seismic Hazard Regions", *Soil Dynamics and Earthquake Engineering*, Vol. 28, pp. 593-604.

Mottershead, J. E. and M. I. Friswell, 1993, "Model Updating in Structural Dynamics: A Survey", *Journal of Sound and Vibration*, Vol. 167, No. 2, pp. 347-375.

Peeters, B., 2000, *System Identification and Damage Detection in Civil Engineering*, Ph.D. Dissertation, Katholieke Universiteit Leuven.

Peeters, B. and G. De Roeck, 1999, "Reference-based Stochastic Subspace Identification for Output-Only Modal Analysis", *Mechanical Systems and Signal Processing*, Vol. 13, No. 6, pp. 855-878.

Richardson, M.H. and D. L. Formenti, 1982, "Parameter Estimation from Frequency Response Measurements using Rational Fraction Polynomials", *Proceedings of the 1st International Modal Analysis Conference*, Florida, USA.

Rytter, A., 1993, *Vibration Based Inspection of Civil Engineering Structures*, Ph.D. Dissertation, Aolborg University.

Scionti, M. and J. Lanslots, 2005, “Stabilization Diagrams: Pole Identification Using Fuzzy Clustering Techniques”, *Advances in Engineering Software*, Vol. 36, pp. 768-779.

Shih, C. Y., Y. G. Tsuei, R. J. Allemang and D. L. Brown, 1988, “Complex Mode Indicator Function and Its Application to Spatial Domain Parameter Estimation”, *Mechanical Systems and Signal Processing*, Vol. 2, No. 4, pp. 367-377. Söderström, T. and P. Stoica, 1989, *System Identification*, Prentice Hall International, London.

Trifunac, M.D., 1972, “Comparison Between Ambient and Forced Vibration Experiments”, *Earthquake Engineering and Structural Dynamics*, Vol.1, p.133-150, 1972

Van Overschee, P. and B. De Moor, 1993, “Subspace Algorithms for the Stochastic Identification Problem”, *Automatica*, Vol. 29, No. 3, pp. 649-660.

Van Overschee, P. and B. De Moor, 1994, “N4SID: Subspace Algorithms for the Identification of Combined Deterministic-Stochastic Systems”, *Automatica*, Vol. 30, No. 3, pp. 75-93.

Viberg, M., 1995, “Subspace-Based Methods for the Identification of Linear Time-Invariant Systems”, *Automatica*, Vol. 31, No. 12, pp.1835-1853.